Table 2 (Continued)

Chromosome	*Start peak*	*End peak*	*hgnc_symbol*	*Description*
5	172672295	172672844		Y RNA [Source:RFAM;Acc:RF00019]
2	177027180	177027529	HOXD4	Homeobox D4 [Source:HGNC Symbol;Acc:5138]
4	85402627	85403376	NKX6-1	NK6 homeobox 1 [Source:HGNC Symbol;Acc:7839]
15	96911497	96912071	MIR1469	MicroRNA 1469 [Source:HGNC Symbol;Acc:35378]
15	89949372	89949871	MIR9-3	MicroRNA 9-3 [Source:HGNC Symbol;Acc:31646]
3	50377447	50378846	RASSF1A [a]	Ras association (RalGDS/AF-6) domain family member 1 [Source:HGNC Symbol;Acc:9882]

[a]Indicates a previously validated gene with a lower threshold for normal tissues than used for the other regions.

endonuclease, either *Bst*UI or *Taq*I, which recognize the sequences 5′-CGCG-3′ or 5′TCGA-3′, respectively. The cytosines in unmethylated restriction sites are converted by sodium bisulfite, amplified by PCR and resist digestion, whereas methylated sites remain unchanged and are cleaved by these enzymes. The digested fragments visualized on agarose gels are thus indicative of methylated restriction sites in the region analyzed. We performed extensive validation analysis by COBRA to confirm the tumor-specific methylated regions (Supplementary Figure 4). Representative examples of COBRA results are shown for the genes *DMRTA2, MIR-129-2* and *GALNTL1*. In total, we inspected the methylation status of 11 genes (*GALNTL1, MIR-10A, MIR-129-2, MIR-196A2, MIR-615, MIR-9-3, AMBRA1, HOXD10, PROX1, ZNF672* and *DMRTA2*) based on the various degrees of methylation obtained from the list of differentially methylated targets. Results for all the targets are presented in Supplementary Table 6. The COBRA analysis revealed that our microarray analysis is highly reliable with over 93% accuracy and only ~4% false negative and ~3% false positive hits.

To further confirm the COBRA results of the methylated genes *GALNTL1* and *DMRAT2*, we sequenced bisulfite-converted DNA from SCLC tumor and matched normal lung samples (Supplementary Figure 4). Normal control lung DNA samples showed either no or very low levels of methylation across the CpG dinucleotides tested in contrast to SCLC tumor DNA samples, which were heavily methylated.

Gene expression and methylation status

For the SCLC cell lines SW1271, H1836 and H1688, and HBECs, Affymetrix gene expression analysis was performed and hypermethylated regions in the SCLC cell lines were compared with their associated probe expression changes. On a global level, we could not detect a correlation between the tumor-specific hypermethylated regions and downregulation of associated genes. This phenomenon has been observed in other tumor methylation studies. Some of the reasons for this lack of correlation are that (1) genes that become methylated in tumors frequently are already expressed at very low levels in corresponding normal tissues,[29–32] (2) methylation-independent mechanisms (such as chromatin modifications) are responsible for expression changes[33] and (3) methylation of alternative promoters obscures such correlations.[27,34] Unlike the methylation patterns, the expression signals of the individual tumor cell lines were not highly correlated to each other when compared with the control cell line (as seen by principal component analysis; data not shown).

Functional pathway analysis of methylated genes

For the two stringencies that were defined ($\geqslant$6 out of 18 tumors specifically hypermethylated and $\geqslant$14 out of 18 tumors specifically hypermethylated), we performed a functional annotation clustering, for promoter proximal tumor-specifically methylated regions and gene body-associated tumor-specifically methylated regions. For $\geqslant$6 out of 18 tumor-specific promoter proximal methylated regions, two main annotation clusters could be identified, one for homeobox genes (*P*-value 1.6E − 26, Bonferroni corrected) and one for transcription factors in general (1.0E − 09; Figure 2a; Supplementary Table 7). More specifically, clusters for neuronal fate commitment (1.3E − 5), neuronal differentiation (3.5E − 9) and pattern specification processes (2.3E − 11) showed the strongest enrichment. In comparison, hypermethylated regions in gene bodies showed similar functional enrichment clusters for homeobox genes (6.2E − 26) and pattern specification processes (3.8E − 11), but significantly less enrichment for neuronal fate commitment (7.0E − 1) and for neuronal differentiation (1.2E − 4; Supplementary Table 8), suggesting that the latter functional categories are more related to promoter-specific methylation (Figure 2a).

Concerning functional enrichment for tumor-specifically hypermethylated regions for the majority of tumors ($\geqslant$14 out of 18 tumors), clusters with significantly less enrichment compared with their less significant counterpart ($\geqslant$6 out of 18) could only be obtained for homeobox genes (7.5E − 7 for promoter regions and 2.3E − 8 for gene bodies) and transcription factors (2.8E − 4 for promoter regions and 3.6E − 2 for gene bodies), which can be partly explained by the lower number of genes in this category (Supplementary Tables 9 and 10). Lung development was another significantly enriched category for promoter methylation (Supplementary Table 9).

With regard to the cell lines, genes associated with hypermethylated regions in the five SCLC cell lines compared with the control cell line, homeobox-related functional terms and transcription factor-related terms were significantly enriched only for gene body-associated tumor peaks (4.8E–8 for homeobox genes and 3.0E − 3 for transcription factors, Bonferroni corrected) but the strong enrichment for these categories observed for promoter regions in the tumor tissues was not present for the cell line models (Supplementary Tables 11 and 12). This probably reflects a greater number and higher diversity of methylation events observed in the cell lines.

For targets methylated simultaneously in $\geqslant$14 out of 18 tumors and in $\geqslant$4 out of 5 cell lines (Supplementary Table 13), we again observed an enrichment in the same functional categories. Notably, this group of genes contained a number of genes involved in neuronal or neuroendocrine differentiation, such as EOMES/TBR2, the gene *TAC1*, which encodes the neuropeptide substance P, and *RESP18*, encoding a neuroendocrine-specific protein.

Motif discovery

We next used the *de novo* motif discovery algorithm HOMER[35] to search for sequence patterns that are associated with regions that are specifically methylated in SCLC tumor samples for at least 33% of the tumors and were able to identify a set of nonredundant sequence motifs that were highly enriched in comparison with all non-tumor-specifically methylated regions on the array.

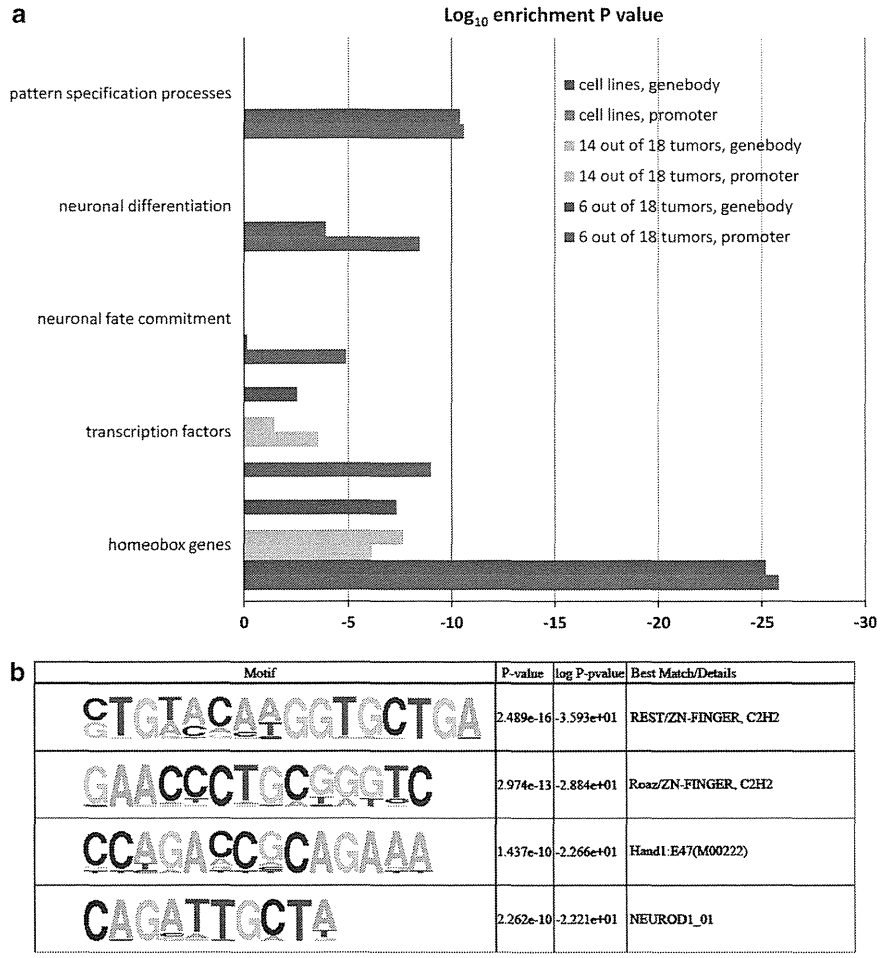

Figure 2. Functional annotation and motif finding analysis. (**a**) Shown are DAVID functional analysis clusters that contained the highest enrichment scores in all three categories: 33% or more of tumors, 77% or more of tumors and cell lines. For more details see Materials and methods. (**b**) Motif finding analysis. Significantly enriched consensus motifs for REST, Roaz/ZNF423, Hand1 and NEUROD1 are shown.

Transcription factors, which were falling into this category, were REST/NRSF (2.5E − 16), ZNF423 (3.0E − 13), HAND1 (1.44E − 10) and NEUROD1 (2.3E − 10; Figure 2b). Examples of methylated NEUROD1 targets are shown in Figure 3. The majority of the sequence motifs identified in methylated regions were enriched within the proximal promoter regions of known genes. The highest enrichment was based on redundant sequence structures and for those that were not, we demanded a stringent alignment with matching transcription factor-binding sites and a low number of occurrences in the background set, which contained all possible methylation sites. REST, ZNF423, HAND1 and NEUROD1 contained nonredundant sequences, a maximal mismatch of 2 bp to the identified *de novo* motif and were selectively enriched in the target sequence set. As such, the identified motifs might not be representative for the whole tumor-specific target set but shed light on sub-regulatory networks with a possibly major impact on the phenotype of SCLC. For example, NEUROD1- and HAND1-binding sites were found in methylated targets representing genes involved in neuronal cell fate commitment such as GDNF, NKX2-2, NKX6-1, EVX1 and SIM2 (Supplementary Tables 2 and 14). Methylation of these binding sites suggests a model in which these transacting factors were lost during tumorigenesis rendering their target sites susceptible to methylation. To analyze this scenario further, we focused on the NEUROD1 transcription factor. Indeed, expression of NEUROD1 proved to be undetectable by a sensitive reverse transcription–PCR assay (Supplementary Figure 5) in the four SCLC cell lines tested and it was expressed at very low levels in human bronchial epithelial cells. In SCLC cell lines and, importantly, also in primary SCLC tumors, the promoter of NEUROD1 was heavily methylated (Supplementary Figures 6A and B) consistent with a possible lack of expression. In addition, we found increased methylation at the promoters of HAND1 and REST in SCLC cell lines and in primary tumors (Supplementary Figure 6).

DISCUSSION

To identify frequently methylated genes in SCLC tumor patients and SCLC cell lines, we have combined the use of a sensitive method for identifying methylation in CpG-rich regions, the MIRA assay[26,27] with genome-wide CpG island and promoter array analysis. Global profiling of 18 SCLC tumor samples compared with normal lung samples resulted in 698 and 73 tumor-specifically methylated and ensembl-annotated gene targets for 33% or more (⩾6 of 18) of tumors, representing a substantial subgroup of patients, and in 77% or more of SCLC tumors (methylation in at least 14 of 18 samples), representing the majority of all patients, respectively. The 73 gene targets methylated in such a large fraction of the patient population may be of particular value for designing DNA methylation-based biomarkers for early detection of SCLC, for example, in serum or sputum, and for disease management.

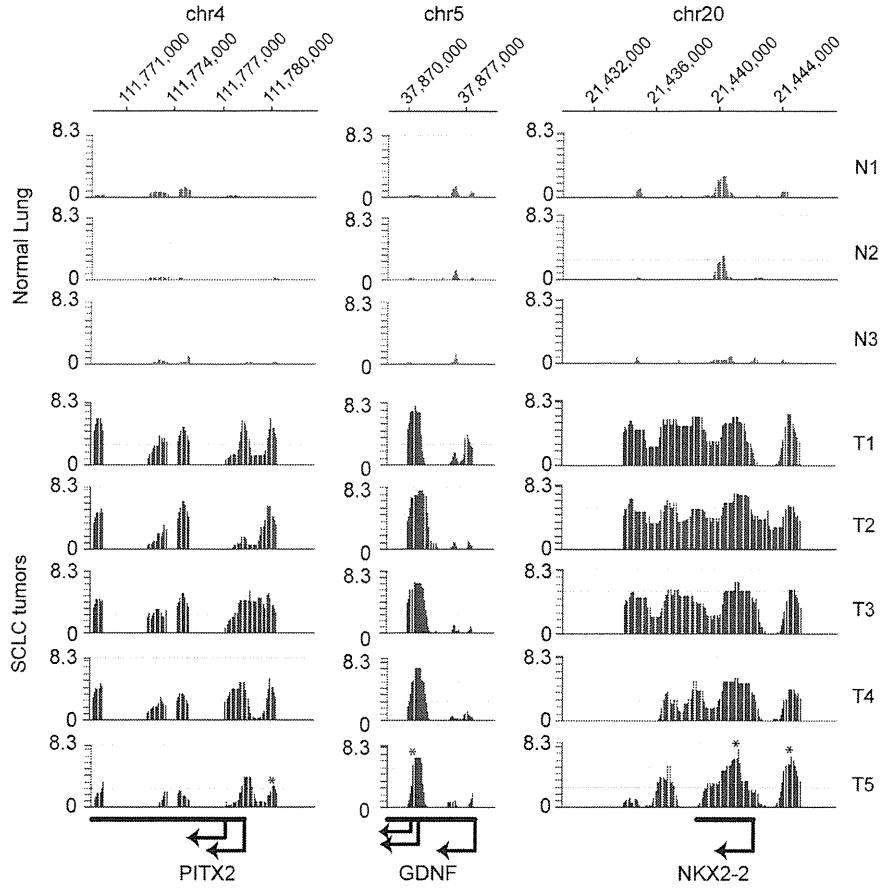

Figure 3. Examples of tumor-specific methylation of NEUROD1 target genes in SCLC. The top of the figure indicates the chromosomal coordinates according to the UCSC Genome browser hg19. Gene names and direction of transcription are shown at the bottom of the figure. The Nimblegen array data (methylated fraction versus input) are shown for three normal lung tissues (red) and five primary SCLC tumors (blue). The methylation signal is shown plotted along the chromosome as a *P*-value score. Therefore, the minimum number on the *y* axis is 0 (when $P = 1$). The *P*-value score was obtained by the NimbleScan software and is derived from the Kolmogorov–Smirnov test comparing the log2 ratios (MIRA versus input) within a 750-bp window centered at each probe and the rest of the data on the array. The asterisks indicate the location of the NEUROD1 target sites.

We randomly selected and validated 11 methylated genomic regions, which were predicted by the array analysis, by using bisulfite-based COBRA assays. The validated targets fell into various major functional categories, including transcription factors and noncoding RNAs such as *GALNTL1, MIR-10A, MIR-129-2, MIR-196A2, MIR-615, MIR-9-3, AMBRA1, HOXD10, PROX1, ZNF672* and *DMRTA2*. Validation of this set of samples revealed the specificity of the analysis. Some of the validated genes are epigenetically altered in various other cancers (*MIR-10A, MIR-129-2, MIR-196A2, HOXD10* and *PROX1*) but other genes have not yet been identified as methylated in any cancer type (*GALNTL1, MIR-615, AMBRA1, ZNF672* and *DMRTA2*). *DMRTA2* methylation was found in 94% of the SCLC tumor patients. The only fact that is known about DMRTA2 is that there is crosstalk of expression with the transcription factor NFIA.[36] Interestingly, there is evidence that NFIA is a key factor for the differentiation of neuronal progenitor cells by downregulating the activity of the Notch signaling pathway via repression of the key Notch effector Hes1.[37] Given the strong enrichment for neuronal differentiation pathways in tumor-specific methylated regions in SCLC (Figure 2) it is tempting to speculate that there is a contribution of DMRTA2 methylation to impaired homeostasis between DMRTA2 and NFIA. There is no functional evidence yet for GALNTL1. These two targets, as well as the many other very frequently methylated genes (Table 2), have the potential to be used as biomarkers for this cancer type.

Gene annotation analysis of tumor-specific promoter methylated targets revealed a substantial subgroup of genes that are specific for neuronal fate commitment, neuronal differentiation and pattern specification processes, along with homeobox and other transcription factors. In comparison, hypermethylated regions in gene bodies showed similar functional enrichment clusters for homeobox genes and pattern specification processes, but significant less enrichment for neuronal fate commitment and for neuronal differentiation, suggesting that the latter functional categories are more specific for promoter-specific methylation. This striking tendency for methylation of neuronal-specific genes may suggest an essential role of this event in SCLC tumor initiation.

Methylation of surrounding proximal promoters is often tightly associated with transcriptional silencing, whereas gene body methylation seems to be associated with transcriptional activation.[27,38] Loss of expression of genes, which are methylated in their proximal promoters, could lead to SCLC tumor initiation. Further studies in this direction will be required to establish experimental evidence. What we do not know at present is whether these genes are unmethylated and expressed in pulmonary neuroendocrine cells and their precursors, the likely cells of origin for SCLC. This specific cell type is currently not available for analysis. This issue does indeed apply to almost all DNA methylation studies done in human cancer to date. The exact

cell of origin, the cell from which the tumor initiates, is often not known, or these cells are not available in sufficient quantities. Therefore—at least theoretically—all DNA methylation 'changes' found in tumor DNA may already preexist in the cell of origin. However, we argue that methylation of genes that promote the differentiation of neuroendocrine cells would be unlikely to occur in such cells as that would interfere with their normal differentiated state.

The SCLC patients investigated in this study showed a strong enrichment of tumor-specific methylation at homeobox genes (Supplementary Tables 15 and 16). Homeobox genes and other transcriptional regulators are important for developmental processes, having important roles in cellular identity, growth, differentiation and cellular interactions within the tissue environment. Given the results of our study, we developed a theory that disruptions in the early phase of these processes would increase the probability of the cell to become malignant, as this would lead to a pool of cells, which are aberrantly kept in a proliferation loop without a decision toward a specific cell fate. As already mentioned, it is thought that the cells of origin for SCLC are neuroendocrine cells, as shown in mice.[10,11] Given the fact that many of the tumor-specifically methylated targets we identified are important for cell fate decisions toward the neuronal lineage, it is intriguing to speculate that one way of shifting the balance toward the emergence of SCLC would be through the repression of key factors critical for differentiation of neuroendocrine cells. One potential way of aberrant shutdown of these critical factors would be by promoter-targeted methylation. Being freed of their normal developmental program by the absence or reduction of cell fate specification factors, some of these cells could acquire additional malignant traits, according to the 'hallmark' model defined by Hanahan and Weinberg.[39] This means that the observed hypermethylated regions are more probable to arise at an early stage of perturbed differentiation rather than during the later stages of tumorigenesis. Concerning other tumor-driving aberrant methylation events, which might increase the tumorigenic potential, it is interesting to note that we could rarely detect any promoter-specific methylation close to known tumor suppressor genes. Exceptions were tumor-specific methylation of *TCF21*,[40] which was detected downstream of the gene in the tumors but overlapping with the TSS in the cell lines and methylation of the promoter of the *RASSF1A* gene confirming earlier gene-specific studies.[17,18]

Another potential way of disrupting cell fate decisions is not by merely reducing the responsible factors but by altering the selectivity toward their genomic recognition sites by aberrant methylation at these regulatory regions, leading to the prevention of binding. Indeed, it has long been known that DNA methylation can prevent transcription factor binding leading to the inhibition of active transcription or the recruitment of methyl-binding proteins, causing gene suppression.[38] When looking for binding sites of important cell fate specificators in our tumor-specific methylated regions, we could indeed identify such a correlation, especially concerning the transcription factors NEUROD1, ZNF423, HAND1 and REST (Figure 2b).

ZNF423 (also known as Ebfaz, Roaz or Zfp423), a gene required for brain development,[41] may also have a role in neuroblastoma. ZNF423 is a transcription factor critically required for cerebellar development and retinoic acid-induced differentiation.[42] Downregulation of ZNF423 expression by RNA interference in neuroblastoma cells results in a growth advantage and resistance to retinoic acid-induced differentiation. Loss of the NF1 tumor suppressor activates RAS-MEK signaling, which in turn represses ZNF423, a critical transcriptional coactivator of the retinoic acid receptors. Neuroblastomas with low levels of both NF1 and ZNF423 have poor clinical outcome.[43]

REST/NRSF is a transcription factor involved in complex regulatory pathways controlling neuronal differentiation,[44] having both oncogenic and tumor-suppressive roles.[45] As shown in several other cancer types, there seems to be a correlation between the level of active REST and the tendency to initiate cancer.[46] Inactivation of the REST/NRSF network may have a role in derepression of some neuroendocrine genes in SCLC.[47] Interestingly, Kreisler *et al.*[48] found that three CpG islands associated with the *REST* gene were methylated in SCLC lines and we also found increased methylation near the *REST* promoter (Supplementary Figure 6). The loss of REST was linked to the malignant progression of SCLC.[48] We present evidence that methylation of *REST*-binding sites might also contribute to the SCLC phenotype.

Given that neuroendocrine cells are the likely cells of origin for SCLC,[10,11] it is interesting that a significant number of NEUROD1 potential binding sites were correlated with methylation in the tumors (Figure 2b). It has been shown in mice that NeuroD deficiency resulted in both impaired alveolar septation and altered morphology of the pulmonary neuroendocrine cells, suggesting a role in the regulation of pulmonary neuroendocrine and alveolar morphogenesis.[49] As such, methylation of NEUROD1-binding sites is supporting our theory of early methylation aberrations causing a defect in the developmental program of pulmonary neuroendocrine cells. Alternatively, lack of expression of transacting developmental transcription factors induced by methylation of their own promoter, which we did find for the *NEUROD1* gene (Supplementary Figure 6), could lead indirectly to methylation of the transcription factor target sites. In this scenario, methylation of the binding site regions of these factors is the default state and can be prevented by *in vivo* binding of the factor. Although hypothetical, our model has gained support from a recent study in mouse ES cells.[50] In this study, it was shown that the presence of several transcription factors, including REST, is required to create genomic regions with low DNA methylation.

In summary, we propose that probably both mechanisms, loss of key transcription factors involved in cell fate decisions or differentiation by methylation of their promoters, and functional inactivation of their corresponding binding site regions by methylation, can guide the cell of origin toward a malignant state. We note that this could be a potential explanation not only for the origin of SCLC but also for tumorigenesis in general.

MATERIALS AND METHODS

Tissue and DNA samples

Primary SCLC tumor tissue DNAs were obtained from patients undergoing surgery at the Nagoya University Hospital or Aichi Cancer Center, Nagoya, Japan. Pairs of human primary SCLC tumor tissue DNA and adjacent normal lung tissue DNA were obtained from Asterand (Detroit, MI, USA), BioChain (Hayward, CA, USA) and Cureline (South San Francisco, CA, USA). SCLC cell lines (H1688, H1417, H1836, DMS53 and SW1271) were obtained from the ATCC (Manassas, VA, USA). The ATCC used short tandem repeat profiling for cell line identification. Normal bronchial epithelial cells (HBECs obtained from Lonza, Walkersville, MD, USA) were used as a control for the cell line analysis. All cells were cultured with Dulbecco's modified Eagle's medium/F12 with 0.5% fetal bovine serum and the bronchial epithelial growth medium bullet kit (Lonza). DNA and RNA from the cell lines were extracted using the DNeasy Blood and Tissue Kit and RNeasy Mini Kit (Qiagen, Valencia, CA, USA), respectively.

MIRA and microarray hybridization

Tumor and normal tissue DNA was fragmented by sonication to ~500 bp average size as verified on agarose gels. Enrichment of the methylated double-stranded DNA fraction by MIRA was performed as described previously.[26,27] The labeling of amplicons, microarray hybridization and scanning were performed according to the NimbleGen (Madison, WI, USA) protocol. NimbleGen tiling arrays were used for hybridization (Human 3 × 720K CpG Island Plus RefSeq Promoter Arrays). These arrays cover all UCSC Genome Browser annotated CpG islands (total of 27 728) as well as the promoters (total of 22 532) of the well-characterized RefSeq genes derived from the UCSC RefFlat files. The promoter region covered is ~3 kb (−2440 to +610 relative to the transcription start sites). For all samples,

the MIRA-enriched DNA was compared with the input DNA. All microarray data sets have been deposited into the NCBI GEO database (accession number GSE35341).

Identification and annotation of methylated regions

Analysis of the arrays was performed with R version 2.10, Perl scripts and the Bioconductor package Ringo.[28] Arrays were clustered in normal tissues, cell lines and tumor tissues using hclust and Spearman's correlation. Biological replicates were quantile-normalized and arrays were normalized by Nimblegen's recommended method, tukey's biweight. Probe ratios were smoothed for three neighboring probes before peak calling. Instead of estimating a cutoff ratio based on a hypothetical normal distribution for non-bound probes (Ringo), a quantile-based approach was chosen to estimate methylation intensities. For this aim, peaks at different quantiles were called, where four probes were above the quantile-based threshold with a distance cutoff of 300 bp. A randomized set of peaks was validated by COBRA assays[51] for each quantile range. Thus, a quantile range of 80% was chosen as a cutoff for methylated regions (defined as hypermethylated regions). False positives and false negatives were assessed by COBRA. To investigate whether inter-sample differences had an influence on the acquired cutoff, predicted peaks were validated in different tissues by COBRA analysis.

Tumor-specific regions were defined using two different stringencies. In one case, an overlap of peaks in 6 or more out of 18 tumor samples (33%) was required above the cutoff quantile threshold of 80%; the genomic regions were defined and for those regions only one out of five normal tissues was allowed to overlap with a peak called on a 56% basis, which resulted in an at least 1.5 ratio change. Overlaps were calculated using BEDtools.[52] A more stringent analysis required an overlap of peaks in at least 14 out of 18 tumors (>77%), with the same settings as above. The obtained chromosomal positions were converted to the latest hg19 genome build, using LiftOver from UCSC, requiring a minimum ratio of 0.9 of bases that must remap. The obtained positions where then annotated using the Bioconductor package ChIPpeakAnno and the latest ensembl annotation from BioMart (Sanger Institute, Cambridge, UK).

Microarray expression analysis

Affymetrix (Santa Clara, CA, USA) human U133plus2.0 arrays for the three cell lines SW1271, H1836 and H1688 were processed by the robust multi-array average method implemented in the Bioconductor 'Affy' package, and the average log2 intensity of each gene across all samples was calculated. The three cell lines were clustered and compared against the control cell line, HBECs. Single expression values were obtained, using the MAS 5.0 method. Proximal promoter hypermethylated and non-hypermethylated regions, defined as -2000 to $+1000$ bp relative to transcription start sites according to the NimbleGen tilling arrays, were assigned with their respective expression probe changes of the corresponding transcript. The correlation between methylation and gene expression was based on a binary decision, linking gene promoters with differentially methylated regions with gene expression changes. A comparison with gene expression changes, where the promoter regions had a change in their methylation level (as measured by peak detected or absent), was above the significance threshold (*P*-value 0.05, two-sided *t*-test).

De novo motif prediction

Motif analysis was performed by HOMER, a program developed by Heinz *et al.*[35] More specifically, the discovery was performed using a comparative algorithm similar to those previously described by Linhart *et al.*[53] Briefly, sequences were divided into target and background sets for each application of the algorithm (choice of target and background sequences are noted below). Background sequences were then selectively weighted to equalize the distributions of CpG content in target and background sequences to avoid comparing sequences of different general sequence content. Motifs of length 8–30 bp were identified separately by first exhaustively screening all possible oligos for enrichment in the target set compared with the background set by assessing the number of target and background sequences containing each oligo and then using the cumulative hypergeometric distribution to score enrichment. Up to two mismatches were allowed in each oligonucleotide sequence to increase the sensitivity of the method. The top 200 oligonucleotides of each length with the best enrichment scores were then converted into basic probability matrices for further optimization. HOMER then generates motifs comprised of a position-weight matrix and detection threshold by empirically adjusting motif parameters to maximize the enrichment of motif instances in target sequences versus background sequences using the cumulative hypergeometric distribution as a scoring function. Probability matrix optimization follows a local hill-climbing approach that weights the contributions of individual oligos recognized by the motif to improve enrichment, while optimization of motif detection thresholds were performed by exhaustively screening degeneracy levels for maximal enrichment during each iteration of the algorithm. Once a motif is optimized, the individual oligos recognized by the motif are removed from the data set to facilitate the identification of additional motifs. Sequence logos were generated using WebLOGO (http://weblogo.berkeley.edu/). Motifs obtained from Jasper and TRANSFAC for which no high-throughput data exists were discarded for this analysis. Only those motifs with the highest alignments to known transcription factors, nonredundant matrixes and non-repetitive sequences were chosen for further analysis.

Functional annotation analysis

Gene ontology analysis was performed using DAVID functional annotation tools with Biological Process FAT and Molecular Function FAT data sets.[54,55] The enriched gene ontology terms were reported as clusters to reduce redundancy. The *P*-value for each cluster is the geometric mean of the *P*-values for all the GO categories in the cluster. The gene list in each cluster contains the unique genes pooled from the genes in all the GO categories in the cluster. Functional terms were clustered by using a Multiple Linkage Threshold of 0.5 and Bonferroni corrected *P*-values.

DNA methylation analysis using sodium bisulfite-based methods

DNA was treated and purified with the EZ DNA Methylation-Gold Kit (Zymo Research, Irvine, CA, USA). PCR primer sequences for amplification of specific gene targets in bisulfite-treated DNA are shown in Supplementary Table 17. The PCR products were analyzed by COBRA as described previously.[51] In addition, PCR products from bisulfite-converted DNA were cloned into pCR2.1-TOPO using a TOPO TA cloning kit (Invitrogen, Carlsbad, CA, USA), and individual clones were sequenced with M13 forward (-20) primer.

Transfection, reverse transcription and quantitative real-time PCR

The DMS53 SCLC line was transfected with a NEUROD1 expression plasmid (2 μg) at ~60% confluence in 35-mm dishes with FuGENE HD (Roche Applied Science, Indianapolis, IN, USA) in serum-free medium according to the manufacturer's recommendations. The cells were cultured for an additional 48 h for analysis of *NEUROD1* expression. Total RNA was isolated from HBECs, all five SCLC cell lines and from DMS53 cells overexpressing *NEUROD1* using the RNeasy Mini Kit (Qiagen). cDNA was prepared using the iScript cDNA synthesis kit (Bio-Rad; Hercules, CA, USA). Quantitative PCR was performed to assess expression of *NEUROD1* and 18S RNA using NEUROD1 primers (forward, 5′-GTTCTCAGGACGAGGAGCAC-3′and reverse 5′-CTTGGGCTTTTGATCGTCAT-3′) and 18S primers (forward 5′-GTAACCC GTTGAACCCCATT-3′ and reverse 5′-CCATCCAATCGGTAGTAGCG-3′). Real-time PCR was performed using iQ SYBR Green Supermix and the iCycler real-time PCR detection system (Bio-Rad). Amplicon expression in each sample was normalized to 18S RNA.

CONFLICT OF INTEREST

Under a licensing agreement between City of Hope and Active Motif (Carlsbad, CA, USA), the MIRA technique was licensed to Active Motif, and the author GPP is entitled to a share of the royalties received by City of Hope from sales of the licensed technology. The rest of the authors declare no conflict of interest.

ACKNOWLEDGEMENTS

We thank Steven Bates for culturing SCLC cell lines. This work was supported by the National Institutes of Health grant CA084469 to GPP and by generous funds from an anonymous donor.

REFERENCES

1 Govindan R, Page N, Morgensztern D, Read W, Tierney R, Vlahiotis A *et al.* Changing epidemiology of small-cell lung cancer in the United States over the last 30 years: analysis of the surveillance, epidemiologic, and end results database. *J Clin Oncol* 2006; **24**: 4539–4544.
2 Wistuba II, Gazdar AF, Minna JD. Molecular genetics of small cell lung carcinoma. *Semin Oncol* 2001; **28**: 3–13.

3 Sekido Y, Fong KM, Minna JD. Molecular genetics of lung cancer. *Annu Rev Med* 2003; **54**: 73–87.
4 Modi S, Kubo A, Oie H, Coxon AB, Rehmatulla A, Kaye FJ. Protein expression of the RB-related gene family and SV40 large T antigen in mesothelioma and lung cancer. *Oncogene* 2000; **19**: 4632–4639.
5 Johnson BE, Ihde DC, Makuch RW, Gazdar AF, Carney DN, Oie H *et al.* myc family oncogene amplification in tumor cell lines established from small cell lung cancer patients and its relationship to clinical status and course. *J Clin Invest* 1987; **79**: 1629–1634.
6 Little CD, Nau MM, Carney DN, Gazdar AF, Minna JD. Amplification and expression of the c-myc oncogene in human lung cancer cell lines. *Nature* 1983; **306**: 194–196.
7 Takahashi T, Obata Y, Sekido Y, Hida T, Ueda R, Watanabe H *et al.* Expression and amplification of myc gene family in small cell lung cancer and its relation to biological characteristics. *Cancer Res* 1989; **49**: 2683–2688.
8 Sattler M, Salgia R. Molecular and cellular biology of small cell lung cancer. *Semin Oncol* 2003; **30**: 57–71.
9 Fischer B, Marinov M, Arcaro A. Targeting receptor tyrosine kinase signalling in small cell lung cancer (SCLC): what have we learned so far? *Cancer Treat Rev* 2007; **33**: 391–406.
10 Sutherland KD, Proost N, Brouns I, Adriaensen D, Song JY, Berns A. Cell of origin of small cell lung cancer: inactivation of Trp53 and rb1 in distinct cell types of adult mouse lung. *Cancer Cell* 2011; **19**: 754–764.
11 Park KS, Liang MC, Raiser DM, Zamponi R, Roach RR, Curtis SJ *et al.* Characterization of the cell of origin for small cell lung cancer. *Cell Cycle* 2011; **10**: 2806–2815.
12 Sato M, Shames DS, Gazdar AF, Minna JD. A translational view of the molecular pathogenesis of lung cancer. *J Thorac Oncol* 2007; **2**: 327–343.
13 Dammann R, Li C, Yoon JH, Chin PL, Bates S, Pfeifer GP. Epigenetic inactivation of a RAS association domain family protein from the lung tumour suppressor locus 3p21.3. *Nat Genet* 2000; **25**: 315–319.
14 Lerman MI, Minna JD. The 630-kb lung cancer homozygous deletion region on human chromosome 3p21.3: identification and evaluation of the resident candidate tumor suppressor genes. The International Lung Cancer Chromosome 3p21.3 Tumor Suppressor Gene Consortium. *Cancer Res* 2000; **60**: 6116–6133.
15 Laird PW. The power and the promise of DNA methylation markers. *Nat Rev Cancer* 2003; **3**: 253–266.
16 Ushijima T. Detection and interpretation of altered methylation patterns in cancer cells. *Nat Rev Cancer* 2005; **5**: 223–231.
17 Burbee DG, Forgacs E, Zochbauer-Muller S, Shivakumar L, Fong K, Gao B *et al.* Epigenetic inactivation of RASSF1A in lung and breast cancers and malignant phenotype suppression. *J Natl Cancer Inst* 2001; **93**: 691–699.
18 Dammann R, Takahashi T, Pfeifer GP. The CpG island of the novel tumor suppressor gene RASSF1A is intensely methylated in primary small cell lung carcinomas. *Oncogene* 2001; **20**: 3563–3567.
19 Sunaga N, Miyajima K, Suzuki M, Sato M, White MA, Ramirez RD *et al.* Different roles for caveolin-1 in the development of non-small cell lung cancer versus small cell lung cancer. *Cancer Res* 2004; **64**: 4277–4285.
20 Kalari S, Pfeifer GP. Identification of driver and passenger DNA methylation in cancer by epigenomic analysis. *Adv Genet* 2010; **70**: 277–308.
21 Rauch TA, Pfeifer GP. DNA methylation profiling using the methylated-CpG island recovery assay (MIRA). *Methods* 2010; **52**: 213–217.
22 Rauch TA, Zhong X, Wu X, Wang M, Kernstine KH, Wang Z *et al.* High-resolution mapping of DNA hypermethylation and hypomethylation in lung cancer. *Proc Natl Acad Sci USA* 2008; **105**: 252–257.
23 Wu X, Rauch TA, Zhong X, Bennett WP, Latif F, Krex D *et al.* CpG island hypermethylation in human astrocytomas. *Cancer Res* 2010; **70**: 2718–2727.
24 Rauch T, Wang Z, Zhang X, Zhong X, Wu X, Lau SK *et al.* Homeobox gene methylation in lung cancer studied by genome-wide analysis with a microarray-based methylated CpG island recovery assay. *Proc Natl Acad Sci USA* 2007; **104**: 5527–5532.
25 Tommasi S, Karm DL, Wu X, Yen Y, Pfeifer GP. Methylation of homeobox genes is a frequent and early epigenetic event in breast cancer. *Breast Cancer Res* 2009; **11**: R14.
26 Rauch TA, Pfeifer GP. The MIRA method for DNA methylation analysis. *Methods Mol Biol* 2009; **507**: 65–75.
27 Rauch TA, Wu X, Zhong X, Riggs AD, Pfeifer GP. A human B cell methylome at 100-base pair resolution. *Proc Natl Acad Sci USA* 2009; **106**: 671–678.
28 Toedling J, Skylar O, Krueger T, Fischer JJ, Sperling S, Huber W. Ringo—an R/Bioconductor package for analyzing ChIP-chip readouts. *BMC Bioinformatics* 2007; **8**: 221.
29 Hahn MA, Hahn T, Lee DH, Esworthy RS, Kim BW, Riggs AD *et al.* Methylation of polycomb target genes in intestinal cancer is mediated by inflammation. *Cancer Res* 2008; **68**: 10280–10289.
30 Reinert T, Modin C, Castano FM, Lamy P, Wojdacz TK, Hansen LL *et al.* Comprehensive genome methylation analysis in bladder cancer: identification and validation of novel methylated genes and application of these as urinary tumor markers. *Clin Cancer Res* 2011; **17**: 5582–5592.
31 Rodriguez J, Munoz M, Vives L, Frangou CG, Groudine M, Peinado MA. Bivalent domains enforce transcriptional memory of DNA methylated genes in cancer cells. *Proc Natl Acad Sci USA* 2008; **105**: 19809–19814.
32 Takeshima H, Yamashita S, Shimazu T, Niwa T, Ushijima T. The presence of RNA polymerase II, active or stalled, predicts epigenetic fate of promoter CpG islands. *Genome Res* 2009; **19**: 1974–1982.
33 Kondo Y, Shen L, Cheng AS, Ahmed S, Boumber Y, Charo C *et al.* Gene silencing in cancer by histone H3 lysine 27 trimethylation independent of promoter DNA methylation. *Nat Genet* 2008; **40**: 741–750.
34 Maunakea AK, Nagarajan RP, Bilenky M, Ballinger TJ, D'Souza C, Fouse SD *et al.* Conserved role of intragenic DNA methylation in regulating alternative promoters. *Nature* 2010; **466**: 253–257.
35 Heinz S, Benner C, Spann N, Bertolino E, Lin YC, Laslo P *et al.* Simple combinations of lineage-determining transcription factors prime cis-regulatory elements required for macrophage and B cell identities. *Mol Cell* 2010; **38**: 576–589.
36 Lee NH, Haas BJ, Letwin NE, Frank BC, Luu TV, Sun Q *et al.* Cross-talk of expression quantitative trait loci within 2 interacting blood pressure quantitative trait loci. *Hypertension* 2007; **50**: 1126–1133.
37 Piper M, Barry G, Hawkins J, Mason S, Lindwall C, Little E *et al.* NFIA controls telencephalic progenitor cell differentiation through repression of the Notch effector Hes1. *J Neurosci* 2010; **30**: 9127–9139.
38 Suzuki MM, Bird A. DNA methylation landscapes: provocative insights from epigenomics. *Nat Rev Genet* 2008; **9**: 465–476.
39 Hanahan D, Weinberg RA. Hallmarks of cancer: the next generation. *Cell* 2011; **144**: 646–674.
40 Smith LT, Lin M, Brena RM, Lang JC, Schuller DE, Otterson GA *et al.* Epigenetic regulation of the tumor suppressor gene TCF21 on 6q23-q24 in lung and head and neck cancer. *Proc Natl Acad Sci USA* 2006; **103**: 982–987.
41 Warming S, Rachel RA, Jenkins NA, Copeland NG. Zfp423 is required for normal cerebellar development. *Mol Cell Biol* 2006; **26**: 6913–6922.
42 Huang S, Laoukili J, Epping MT, Koster J, Holzel M, Westerman BA *et al.* ZNF423 is critically required for retinoic acid-induced differentiation and is a marker of neuroblastoma outcome. *Cancer Cell* 2009; **15**: 328–340.
43 Holzel M, Huang S, Koster J, Ora I, Lakeman A, Caron H *et al.* NF1 is a tumor suppressor in neuroblastoma that determines retinoic acid response and disease outcome. *Cell* 2010; **142**: 218–229.
44 Qureshi IA, Gokhan S, Mehler MF. RESTand CoREST are transcriptional and epigenetic regulators of seminal neural fate decisions. *Cell Cycle* 2010; **9**: 4477–4486.
45 Majumder S. REST in good times and bad: roles in tumor suppressor and oncogenic activities. *Cell Cycle 2006;* **5**: 1929–1935.
46 Coulson JM. Transcriptional regulation: cancer, neurons and the REST. *Curr Biol* 2005; **15**: R665–R668.
47 Coulson JM, Edgson JL, Woll PJ, Quinn JP. A splice variant of the neuron-restrictive silencer factor repressor is expressed in small cell lung cancer: a potential role in derepression of neuroendocrine genes and a useful clinical marker. *Cancer Res* 2000; **60**: 1840–1844.
48 Kreisler A, Strissel PL, Strick R, Neumann SB, Schumacher U, Becker CM. Regulation of the NRSF/REST gene by methylation and CREB affects the cellular phenotype of small-cell lung cancer. *Oncogene* 2010; **29**: 5828–5838.
49 Neptune ER, Podowski M, Calvi C, Cho JH, Garcia JG, Tuder R *et al.* Targeted disruption of NeuroD, a proneural basic helix-loop-helix factor, impairs distal lung formation and neuroendocrine morphology in the neonatal lung. *J Biol Chem* 2008; **283**: 21160–21169.
50 Stadler MB, Murr R, Burger L, Ivanek R, Lienert F, Scholer A *et al.* DNA-binding factors shape the mouse methylome at distal regulatory regions. *Nature* 2011; **480**: 490–495.
51 Xiong Z, Laird PW. COBRA: a sensitive and quantitative DNA methylation assay. *Nucleic Acids Res* 1997; **25**: 2532–2534.
52 Quinlan AR, Hall IM. BEDTools: a flexible suite of utilities for comparing genomic features. *Bioinformatics* 2010; **26**: 841–842.
53 Linhart C, Halperin Y, Shamir R. Transcription factor and microRNA motif discovery: the Amadeus platform and a compendium of metazoan target sets. *Genome Res* 2008; **18**: 1180–1189.
54 Huang da W, Sherman BT, Lempicki RA. Systematic and integrative analysis of large gene lists using DAVID bioinformatics resources. *Nat Protoc* 2009; **4**: 44–57.
55 Huang da W, Sherman BT, Lempicki RA. Bioinformatics enrichment tools: paths toward the comprehensive functional analysis of large gene lists. *Nucleic Acids Res* 2009; **37**: 1–13.

Supplementary Information accompanies the paper on the Oncogene website (http://www.nature.com/onc)

doi: 10.1111/j.1472-8206.2012.01056.x

ORIGINAL ARTICLE

Thymoquinone as an anticancer agent: evidence from inhibition of cancer cells viability and invasion in vitro and tumor growth *in vivo*

Samir Attoub[a]*, Olivier Sperandio[b], Haider Raza[c], Kholoud Arafat[a], Suhail Al-Salam[d], Mahmood Ahmed Al Sultan[a], Maha Al Safi[a], Takashi Takahashi[e] and Abdu Adem[a]

[a]*Department of Pharmacology & Therapeutics, Faculty of Medicine & Health Sciences, United Arab Emirates University, PO Box: 17666, Al Ain, United Arab Emirates*

[b]*INSERM UMR-S973/MTi, Université Paris Diderot, Bâtiment Lamarck, 35 Rue Hélène Brion, 75205 Paris Cedex 13, France*

[c]*Department of Biochemistry, Faculty of Medicine & Health Sciences, United Arab Emirates University, PO Box 17666, Al Ain, United Arab Emirates*

[d]*Department of Pathology,Faculty of Medicine & Health Sciences, UAE University, PO Box 17666, Al Ain, United Arab Emirates*

[e]*Division of Molecular Carcinogenesis, Center for Neurological Diseases and Cancer, Nagoya University Graduate School of Medicine, 65 Tsurumai-cho, Showa-ku, Nagoya, 466-8550, Japan*

Keywords
DNA damage,
invasion,
lung & breast cancer,
thymoquinone,
tumor growth,
viability

Received 11 March 2012;
revised 9 May 2012;
accepted 4 June 2012

*Correspondence and reprints:
samir.attoub@uaeu.ac.ae

ABSTRACT

Phytochemical compounds are emerging as a new generation of anticancer agents with limited toxicity in cancer patients. The purpose of this study was to investigate the potential impact of thymoquinone (TQ), the major constituent of black seed, on survival, invasion of cancer cells in vitro, and tumor growth *in vivo*. Exposure of cells derived from lung (LNM35), liver (HepG2), colon (HT29), melanoma (MDA-MB-435), and breast (MDA-MB-231 and MCF-7) tumors to increasing TQ concentrations resulted in a significant inhibition of viability through the inhibition of Akt phosphorylation leading to DNA damage and activation of the mitochondrial-signaling proapoptotic pathway. We provide evidence that TQ at non-toxic concentrations inhibited the invasive potential of LNM35, MDA-MB-231, and MDA-MB231-1833 cancer cells. Moreover, we demonstrate that TQ synergizes with DNA-damaging agent cisplatin to inhibit cellular viability. The anticancer activity of thymoquinone was also investigated in athymic mice inoculated with the LNM35 lung cells. Administration of TQ (10 mg/kg/i.p.) for 18 days inhibited the LNM35 tumor growth by 39% ($P < 0.05$). Tumor growth inhibition was associated with significant increase in the activated caspase-3. The *in silico* target identification suggests several potential targets of TQ mainly HDAC2 proteins and the 15-hydroxyprostaglandin dehydrogenase. In this context, we demonstrated that TQ treatment resulted in a significant inhibition of HDAC2 proteins. In view of the available experimental findings, we contend that thymoquinone and/or its analogues may have clinical potential as an anticancer agent alone or in combination with chemotherapeutic drugs such as cisplatin.

INTRODUCTION

Cancer is a leading cause of death worldwide and remains a therapeutic enigma. Among different forms of cancer, lung cancer is the most common with the highest mortality rate, and colorectal cancer is the second cause of cancer-related death after lung cancer in men and breast cancer in women. Hepatocellular carcinoma is also a common cancer in Asia and Africa and one of the most common causes of cancer-related mortality worldwide, accounting for about half a million deaths annually [1]. Despite advances in molecular biology of cancer, improved diagnosis, and new targeted therapies, the cure of lung, breast, and colon cancer remain elusive. To improve the survival of cancer patients, we need to develop new cytotoxic compounds and make use of selective molecular targeting anticancer drugs.

Over recent years, growing interest in phytochemical compounds with anticancer potential has been observed stimulating more in vitro and preclinical screening of these compounds. Thymoquinone (TQ), the most abundant constituent of black seed (*Nigella Sativa*), has been shown to exert anti-inflammatory, anti-oxidant, and antineoplastic effects both in vitro and *in vivo* [2,3]. TQ has been shown to inhibit cellular proliferation and induce apoptosis in human colon, breast, brain, pancreatic, and ovarian cancer cell lines [3–6]. The numerous reports on the protective effect of thymoquinone against drug-induced toxicity suggest a possible role of thymoquinone as an adjuvant in improving the quality of life of cancer patients [3]. In this study, we investigated the impact of thymoquinone on human cancer cell survival, and invasion in vitro and tumor xenograft growth *in vivo*. Our results showed a dramatic anticancer effect of TQ on a variety of tumor cells under in vitro as well as on lung tumor growth *in vivo*. We have also hypothesized functional targets that may potentially be affected by TQ using *in silico*-based protein data bank.

MATERIALS AND METHODS

Cell culture and reagents

Human lung cancer cells LNM35 (NSCLC) [7] were maintained in RPMI 1640 (Invitrogen, Paisley, UK); human hepatoma cells HepG2, human colorectal cancer cells HT29, human mammary adenocarcinoma cells (MCF-7, MDA-MB-231, and MDA-MB-213-1833), and human melanoma MDA-MB-435 were maintained in DMEM (Invitrogen). All media were supplemented with 10% fetal bovine serum (Roche Molecular Biochemicals, Meylan, France). Thymoquinone was purchased from Sigma-Aldrich (Saint-Quentin Fallavier, France).

Primary antibodies were purchased from the following manufacturers: polyclonal antibodies for cytochrome *c*, poly (ADP-ribose) polymerase (PARP), and HDAC2 (Santa Cruz, CA, USA), Bcl-2, phosphor-Akt (Cellular Signaling Technology, Beverly, MA, USA), phospho-histone H2a.X (Millipore, Hayward, CA, USA), and monoclonal rat anti-mouse CD31 antibody (BD Pharmingen, San Jose, CA, USA). The secondary antibodies were goat anti-rat antibody (Sigma, Saint Louis, MO, USA) and rabbit anti-mouse antibody (Dako, Copenhagen, Denmark). Signal Stain Cleaved Caspase-3 (Asp175) IHC detection kit was purchased from Cellular Signaling Technology).

Cellular viability

Cells were seeded at 5000 cells/well in 96-well plate. After 24 h, cells were treated for another 24 h with increasing concentrations of thymoquinone (1–100 μM) in triplicates. Control cultures were treated with 0.1% DMSO. The effect of thymoquinone on cell viability was determined using a CellTiter-Glo luminescent cell viability assay (Promega Corporation, Madison, WI, USA), based on quantification of ATP, which signals the presence of metabolically active cells. Luminescent signal was measured using GLOMAX Luminometer system. The data were presented as proportional viability (%) by comparing the treated group with the untreated cells, the viability of which is considered as 100%.

Caspase-3/7 activity

Cells were seeded at a density of 5000 cells/well into 96-well plate and treated with 10 μM of thymoquinone (HepG2) and with 100 μM of thymoquinone for 24 h (LNM35), in triplicate assays. Caspase-3/7 activity was measured using a luminescent Caspase-Glo 3/7 assay kit following manufacturer's instructions (Promega Corporation). Caspase reagent was added, and the plate was mixed using an orbital shaker and incubated for 2.5 h at room temperature. Luminescence was measured using a GLOMAX Luminometer system (Promega, Madison, WI, USA).

Expression of apoptotic and DNA damage protein members

LNM35 and MDA-MB-231 cells were seeded in 100 mm dishes at 3×10^6 cells/dish for 24 h and with

increasing concentrations of thymoquinone (1–50 μM) for 30 min, 2, 6, and 24 h. Total cellular proteins were isolated using RIPA buffer (25 mM Tris–HCl pH 7.6, 1% nonidet P-40, 1% sodium deoxycholate, 0.1% SDS, 0.5% protease inhibitors cocktail, 1% PMSF, 1% phosphatase inhibitors cocktail) from control and treated cells. The whole cell lysate was recovered by centrifugation at 23 000 g for 20 min at 4 °C to remove insoluble material, and 50 μg of protein was separated by a 10% SDS gel for phospho-Akt and HDAC2 and 12% SDS gel for Anti-phospho-Histone H_2aX. After electrophoresis, the proteins were transferred on a nitrocellulose membrane, blocked with 5% non-fat milk and probed with $pSer^{473}$-Akt (1 : 1000), H_2aX (1 : 500), HDAC2 (1 : 200), and β-actin (1 : 1000) antibodies overnight at 4 °C. The blot was washed, exposed to horseradish peroxidase (HRP)-conjugated secondary antibodies, and visualized using the ECL system (Santa Cruz).

For the expression of cytochrome *c*, PARP, and Bcl-2, the cells were seeded in 100 mm dishes at 3×10^6 cells/dish and treated with 10 μM of thymoquinone for 6 and 24 h. After, cells were harvested, washed with PBS (pH 7.4), and homogenized in mitochondrial isolation H-medium buffer (70 mM sucrose, 220 mM mannitol, 2.5 mM HEPES, 2 mM EDTA) and 0.1 mM phenylmethylsulfonylfluoride at 4 °C. Mitochondria and postmitochondrial supernatants (PMS) were prepared by centrifugation, and the purity of the mitochondrial fraction was ascertained by assaying for organelle-specific marker enzymes as described previously [8]. Mitochondrial preparations containing <3% cross-contamination were used in experiments. Proteins (50 μg) from mitochondria and PMS were separated on 12% SDS-PAGE and electrophoretically transferred onto nitrocellulose paper by Western blotting. The immunoreacting protein bands were visualized after interacting with primary antibodies against cytochrome *c* and PARP and Bcl-2 as described before [9].

Wound healing motility assay

LNM35 and MDA-MB-231 cells were grown in six-well tissue culture dishes until they reach confluence. A scrape was made through the confluent monolayer with a plastic pipette tip of 1-mm diameter. Afterwards, dishes were washed twice and incubated at 37 °C in fresh RPMI containing 10% fetal calf serum in the presence or absence of the indicated concentrations of thymoquinone (1 and 10 μM). At the bottom side of each dish, two arbitrary places were marked where the width of the wound was measured with an inverted microscope (4×). Motility was expressed as the average ± SEM of the difference between the measurements at time zero and the 2–24 h time period.

Matrigel and Oris invasion assays

The invasiveness of the lung cancer cells LNM35 and breast cancer cells MDA-MB-231 treated with thymoquinone (1 and 10 μM) was tested using BD Matrigel Invasion Chamber (8-μm pore size; BD Biosciences, Le Pont de Claix, France). The PI3′-K inhibitor LY294002 (20 and 50 μM, respectively) was used as a positive inhibitor of cellular invasion. Cells (1×10^5 cells in 0.5 mL of media and the indicated concentration of thymoquinone) were seeded into the upper chambers of the system, and the bottom wells in the system were filled with RPMI supplemented with 10% fetal bovine serum as a chemo-attractant and then incubated at 37 °C for 24 h. Non-penetrating cells were removed from the upper surface of the filter with a cotton swab. Cells that have migrated through the matrigel were fixed with 4% formaldehyde, stained with DAPI, and counted in 20 random fields under a microscope. For quantification, the assay was performed in duplicates and repeated three times.

The Oris™ Cell Invasion Assay (AMS Biotechnology, Abingdon, UK) was used to investigate the impact of thymoquinone on MDA-MB-231-1833 cell invasion in vitro within a 3-dimensional extracellular matrix comprised of a basement membrane extract (BME) of the murine Engelbreth-Holm-Swarm tumor. Cells were seeded at 100 000 cells/well and allowed to attach overnight onto plates coated with BME solution. Once the cells formed a confluent monolayer, the silicone stoppers were removed and the cells treated with thymoquinone (1 and 10 μM) or the PI3′-K inhibitor LY294002 (20 μM). Following 48 h invasion, cells were labeled with Calcein AM (Invitrogen, CA, USA), and images were acquired, in the absence of the mask, by use of an Olympus fluorescence microscope.

Tumor growth and metastasis assay

Six-week-old athymic NMRI female nude mice (nu/nu, Elevage Janvier, France) were housed in filtered-air laminar flow cabinets and handled under aseptic conditions. Procedures involving animals and their care were conducted in conformity with Institutional guidelines that are in compliance with Faculty of

Medicine and Health Sciences, UAEU, National and International laws and policies (EEC Council Directive 86/609, OJ L 358, 1, December 12, 1987; and NIH Guide for Care and Use of Laboratory Animals, NIH Publication No. 85–23, 1985). Human Pulmonary LNM35 cells (1×10^6 cells) were injected subcutaneously into the lateral flank of the nude mice. One week after inoculation, when tumors had reached the volume of approximately 100 mm^3, animals (six in each group) were treated with thymoquinone (10 mg/kg, i.p.) or control (vehicle alone) 3 days per week (Sunday, Tuesday, and Thursday) for a total of 18 days. Tumor dimensions were measured with calipers every 3 days. Tumor volume (V) was calculated using the formula: $V = 0.4 \times a \times b^2$, with '$a$' being the length and '$b$' the width of the tumor. The animals were killed 18 days after treatment initiation, and the tumors and the axillary lymph nodes were excised, weighed, and fixed for immunohistochemical analysis.

Immunohistochemical determination of CD31/platelet-endothelial cell adhesion molecule 1 (PECAM-1) for microvessel density and cleaved caspase-3 for apoptotic cells

The effect of thymoquinone on angiogenesis was evaluated using CD31 immunostaining. The tumor tissues were quickly frozen in isopentane at −130 °C and stored at −70 °C until further processing. The frozen sections (8 μm) were fixed in acetone and incubated overnight with a CD31 antibody (1 : 400). Slides were then washed three times in PBS and incubated with secondary antibody (goat anti-rat 1 : 200) for one hour at room temperature. The sections were then stained with DAB and counterstained with hematoxylin. Vessel density was determined by counting the number of microvessels. The area occupied by CD31-positive microvessels and total tissue area per section were quantified and compared between treated and control mice. For individual tumors, the microvessel count was scored by averaging the counts from all fields. All analyses were performed in a blind fashion. The paraffin-embedded tissue sections (5 μm) were deparaffinized and then microwaved for 5 min for antigen retrieval. For the identification of apoptotic cells, cleaved caspase-3 staining was performed following the instructions of a commercially available Signal Stain Cleaved Caspase-3 (Asp175) IHC detection kit (Cellular SignalingTechnology, Beverly, MA, USA). Ten high-power fields (0.159 mm^2) per section of four to five tumors per treatment group were examined microscopically, and the average number of cells that stained positive for cleaved caspase-3 per treatment group was evaluated.

TarFisDock is a web-based tool for automating the procedure of searching for small molecule–protein interactions over a large repertoire of protein structures. It offers PDTD (potential drug target database), a target database containing 698 protein structures covering 15 therapeutic areas and a reverse ligand–protein docking program [10].

Potential Drug Target Database (PDTD) is a web-accessible protein database for *in silico* target identification. It currently contains >1100 protein entries with 3D structures presented in the Protein Data Bank. Data are extracted from the literatures and several online databases such as TTD, DrugBank, and Thomson Pharma. The database covers diverse information of >830 known or potential drug targets, including protein and active sites' structures in both PDB and mol2 formats, related diseases, biological functions as well as associated regulating (signaling) pathways. Each target is categorized by both nosology and biochemical function. In conjunction with TarFisDock, PDTD can be used to identify binding proteins for small molecules. The results can be downloaded in the form of mol2 file with the binding pose of the probe compound and a list of potential binding targets according to their ranking scores [11].

Statistical analysis

Results were expressed as means ± SEM. The difference between experimental and control values were assessed by ANOVA followed by Dunnett post hoc multiple comparison test. Tumor growth assays were analyzed using the unpaired Student's t-test. $P < 0.05$ indicates a significant difference.

RESULTS

Effect of thymoquinone on cell viability

As shown in *Figure 1*, exposure of LNM35, HepG2, HT29, MDA-MB-435, MDA-MB-231, and MCF-7 cells to increasing TQ concentrations (1–100 μM) for 24 h decreased cellular viability in a concentration-dependent manner. The IC_{50} concentrations (producing half-maximal inhibition) at 24 h were between 50 and 78 μM of TQ for all cells except for HepG2, and the IC_{50} was 34 μM of TQ. HepG2 cells seem to be the more sensitive cells to the cytotoxic effects of thymoquinone.

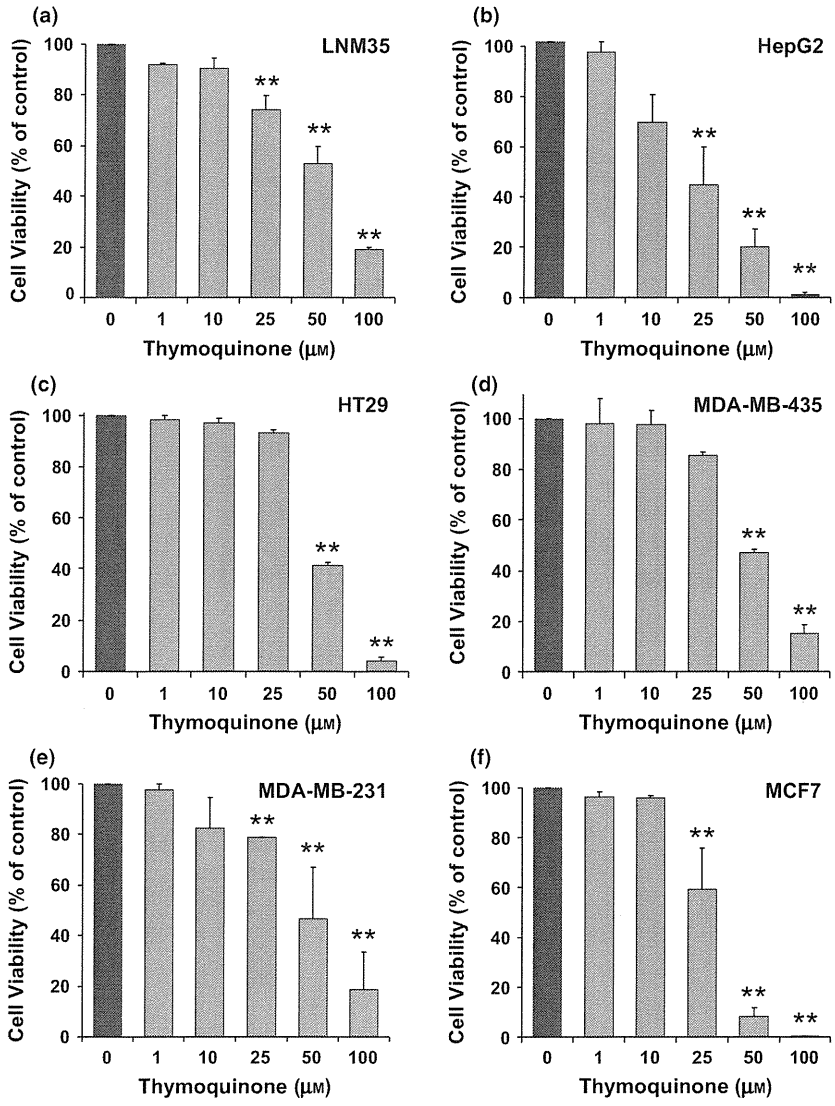

Figure 1 Inhibition of cellular viability by thymoquinone. Exponentially growing LNM35, HepG2, HT29, MDA-MB-435, MDA-MB-231, and MCF7 cells were treated for 24 h with vehicle (0.1% DMSO) and the indicated concentrations of thymoquinone. Viable cells were assayed as described in Materials and Methods. All experiments were repeated at least three times. *Columns*, mean; *bars*, SEM. **Significantly different at $P < 0.01$.

TQ treatment inhibits Akt phosphorylation and induces DNA damage in both MDA-MB-231 and LNM35 cancer cells

Phosphorylated Akt promotes cancer cell survival by inhibiting downstream apoptotic targets, such as proapoptotic Bcl-2 family member BAD and GSK-3 and increasing the survival targets such as Bcl-2. In this context, inhibition of the Akt pathway has been targeted as a promising strategy for cancer therapy. LNM35 and MDA-MB-231 cells were exposed to increasing concentrations of TQ for 30 min, 2, 6, and 24 h and total proteins were evaluated for phosphorylated Akt on serine 473. In both LNM35 and MDA-MB-231 cells, TQ induces a clear concentration and time-dependent inhibition of p-Akt (*Figure 2a*). These results indicate that the induction of apoptosis by TQ is at least in part associated with reduction in activated survival kinase Akt.

To check whether the induction of cell death by TQ is because of DNA damage, LNM35 as well as MDA-MB-231 cells were exposed to increasing concentrations of TQ for 30 min, 2, 6, and 24 h and total proteins were evaluated for γ-H_2aX expression. In both LNM35 and MDA-MB-231 cells, TQ induces a concentration and time-dependent increase in γ-H_2aX expression indicating that cell death induced by TQ was associated with induction of DNA damage (*Figure 2b*).

Cytochrome *c* release from mitochondria, caspase-3/7, and PARP activation

HepG2, the more sensitive cells to the cytotoxic effect of TQ, were used to determine whether the thymoquinone

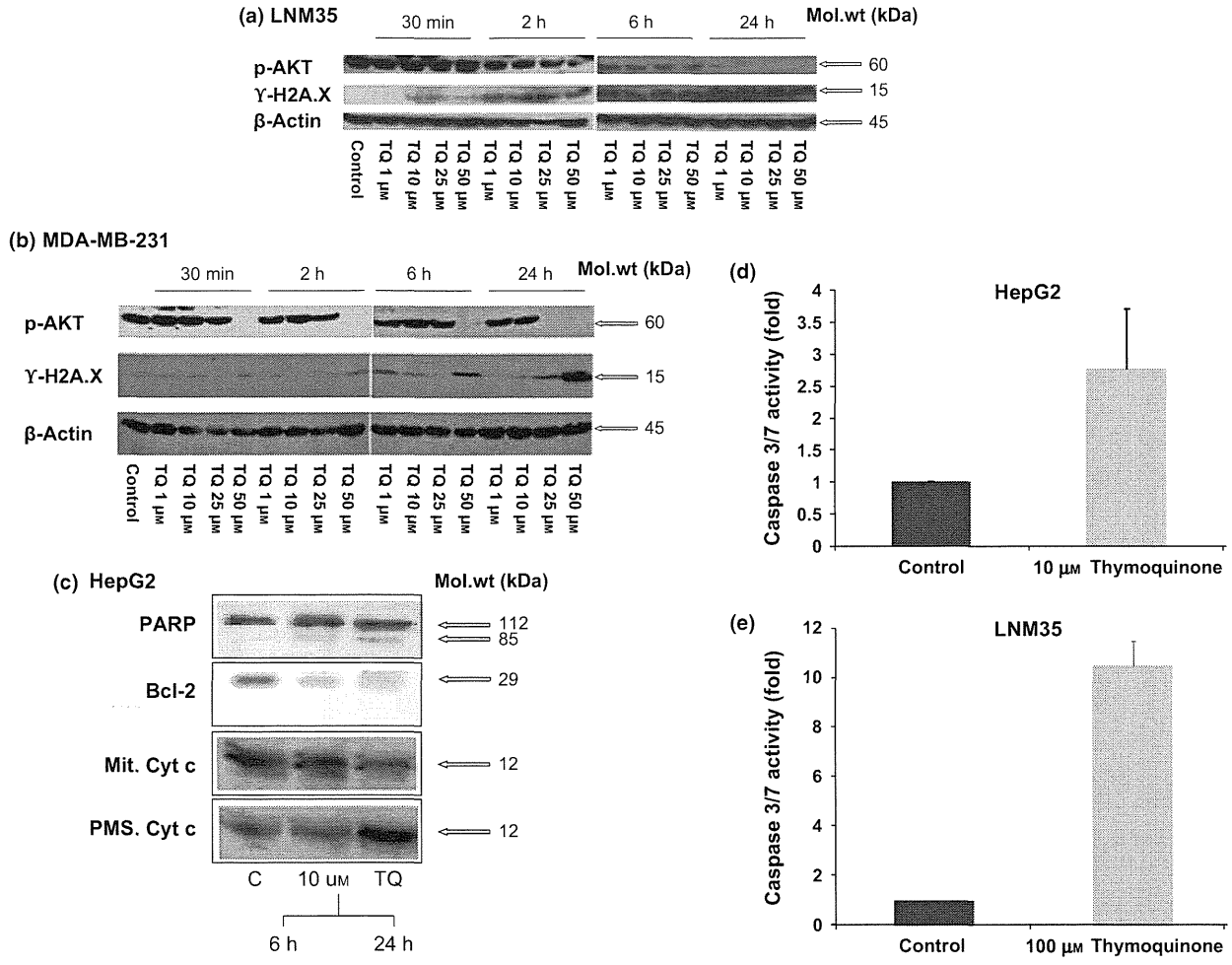

Figure 2 Phosphorylation of Akt and H_2aX, cytochrome *c* release, induction of caspase-mediated apoptosis PARP activation by thymoquinone. Indicated cells were exposed to increasing concentrations of TQ, and total proteins were collected after 30 min, 2, 6, and 24 h, and the phosphorylation of Akt and H_2aX protein was assessed by immunoblot in (a) LNM35 and (b) MDA-MB-231 cells. (c) Human hepatoma cancer cells HepG2 were treated with vehicle (0.1% DMSO) or 10 μM of thymoquinone for 6 h. c, upper panel) PARP cleavage in HepG2 cells treated with thymoquinone 10 μM and incubated for incubated for 6 and 24 h. Cleavage of PARP was detected by Western blotting; 112- and 85-kDa protein bands indicated native and cleaved PARP, respectively. c, lower panel) Cytochrome *c* expression in the mitochondria and postmitochondrial supernatants (PMS). (d) Induction of caspase-3/7 activity by thymoquinone in HepG2 cells and (e) in LNM35 cells. Caspase-3/7 activity was determined using the Caspase-Glo 3/7 assay and was normalized to the number of viable cells per well and expressed as fold induction compared with the control group.

effect was because of apoptosis. Western blot analysis of the HepG2 cells revealed that 6 and 24 h treatment with 10 μM thymoquinone caused an increase in the release of cytochrome *c* from the mitochondria as compared to the control cells (*Figure 2c*). In a sequential manner, once the cytochrome *c* released into cytosol, it recruits and activates caspases that are the executioners of apoptosis. To determine whether cells were undergoing apoptosis, the activity of the main effector caspases, caspases-3 and -7, was analyzed using the Caspase-Glo 3/7 assay 6 h after treatment with TQ (10 μM). The relative caspase activity was normalized to the number of cells per well and compared to the control cells. A significant 2.7 fold increase in caspase-3 and -7 activities was observed in HepG2 cells (*Figure 2d*). To confirm that LNM35 cells also were undergoing apoptosis after exposure to thymoquinone, caspase-3/7 was measured 24 h after treatment with TQ (100 μM). A 10 folds increase in caspase-3/7 activity was observed in LNM35 cells after treatment with TQ

100 μM (*Figure 2e*). Poly-(ADP-ribose) polymerase-1 (PARP-1) is a nuclear enzyme involved in DNA repair and stability downstream of caspase-3/7 activation. Cleavage of PARP-1 is used as a hallmark of caspase-3/7 activation and apoptosis. PARP-1 cleavage during apoptosis impairs the DNA repair capacity of the cell. Intact PARP (112 kDa) was seen in DMSO-treated HepG2 cells. However, after 6 and 24 h treatment of HepG2 cells with 10 μM of thymoquinone, PARP was cleaved into an 85 kDa fragment as a result of caspase-3/7 activation and which is consistent with cell death that results from apoptosis (*Figure 2c*). We also demonstrated a reduced expression of BcL-2 in HepG2 cells after TQ treatment (*Figure 2c*).

Impact of thymoquinone on cancer cell motility and invasion

Using a classic in vitro wound healing model, we assessed whether thymoquinone was able to inhibit epithelial cell motility. Thymoquinone was found to be ineffective in reducing cellular motility in the LNM35 cells (*Figure 3a*); similarly, the dose- and time-dependant inhibition observed in the MDA-MB-231 was also not statistically significant even after 6 h incubation with TQ 10 μM (*Figure 3b*).

However, TQ was able to significantly reduce the invasiveness of both LNM35 and MDA-MB-231 cells in matrigel invasion assay (*Figure 4a,b*). The inhibition of matrigel invasion seen following exposure of cells to low concentrations of TQ (0.1, 1, and 10 μM) occurred

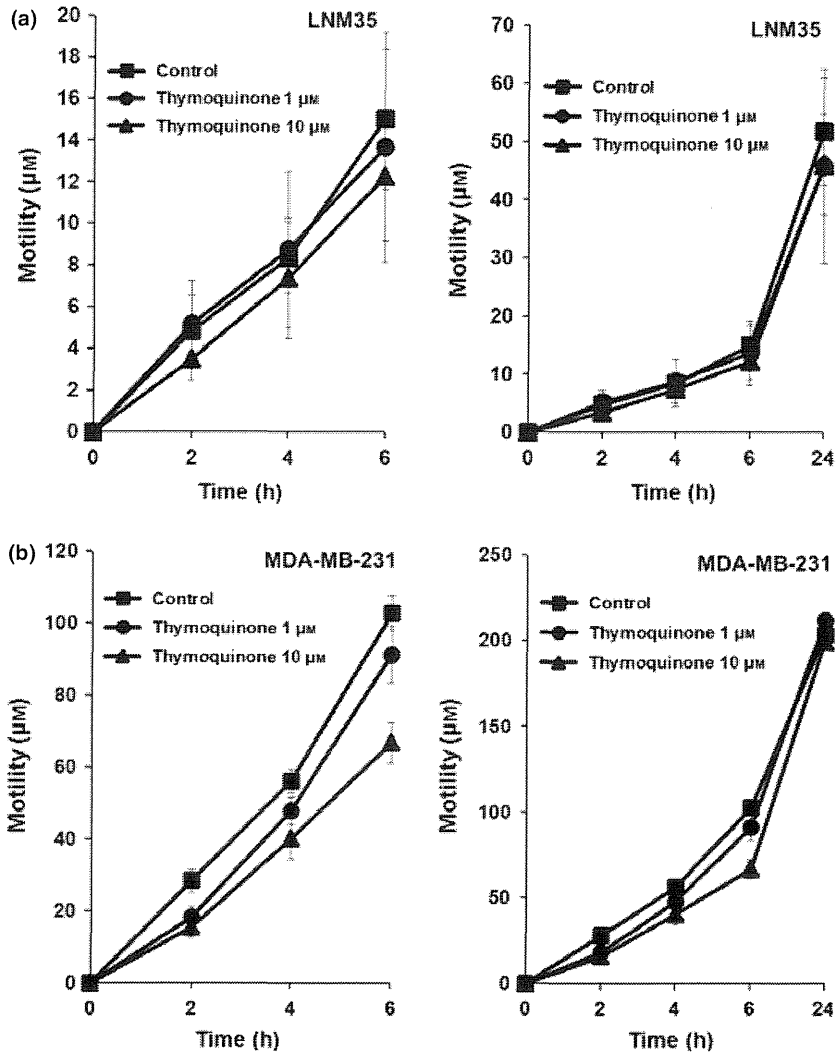

Figure 3 Dose–response effect of thymoquinone on cellular motility. Wounds were introduced in confluent monolayers LNM35 (a) and MDA-MB-231 (b) cells in the presence or absence (control) of thymoquinone (1 and 10 μM). The mean distance that cells travelled from the edge of the scraped area for 2, 4, 6, and 24 h at 37 °C was measured in a blinded fashion, using an inverted microscope (4× magnifications). Data are means ± SEM of two independent experiments.

without reduction in cell viability (*Figure 1a,e*). Next, we investigated the impact of non-toxic concentration of 1 μM of TQ (*Figure 4c*) on the invasiveness of the highly invasive breast cancer cells MDA-MB231-1833 using Oris invasion assay. Again, TQ reduced the invasiveness of these cells at the non-toxic concentration of 1 μM (*Figure 4d*). We conclude that TQ significantly reduced the invasive potential of lung cancer (LNM35) and breast cancer (MDA-MB231 and MDA-MB231-1833) cells.

In vivo impact of thymoquinone on tumor growth

The anticancer activity of TQ was investigated in athymic mice inoculated with the highly tumorigenic LNM35 human lung cells as xenografts. TQ reduced the growth of LNM35 human tumor xenografts by 39% at day 18 (*Figure 5a*). There was no sign of toxicity because of thymoquinone administration and no significant difference in body weight between the thymoquinone-treated animals and the control group (data not shown). The effect of TQ on tumor angiogenesis was assessed by CD31-immunostaining of LNM35 tumor tissue xenografts. CD31 is specifically expressed on the surface of endothelial cells and is weakly expressed on lymphoid cells and platelets. Immunohistochemical analysis indicated that when the CD31-positive areas or number of microvessels was normalized to tumor area, TQ vs. control did not cause vascular regression in the tumors. LNM35 tumor growth inhibition was associated with a significant increase in caspase-3 activity similar to the in vitro results indicating that the tumor growth inhibition induced by TQ is mainly due to the induction of apoptosis (*Figure 5b*). Next, we assessed the metastatic behavior of the human pulmonary cell

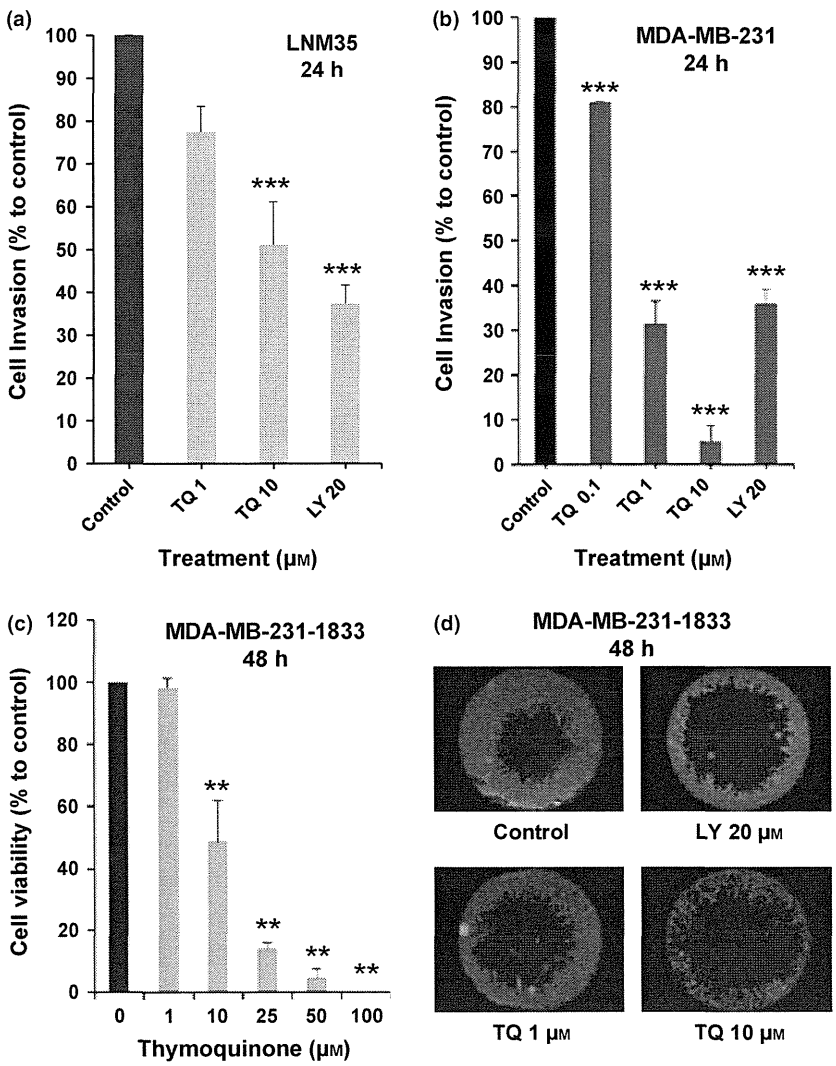

Figure 4 Dose effect of thymoquinone on matrigel and Oris cell invasion assay. (a) LNM35; (b) MDA-MB-231 cells were incubated for 24 h in the presence or absence of thymoquinone (0.1–10 μM). Cells that invaded into matrigel were scored as described in Materials and Methods. *Columns*, mean; bars, SEM. (c) MDA-MB-213-1833 cells were treated with vehicle for 48 h (0.1% DMSO) and the indicated concentrations of TQ. Viable cells were assayed as described in Materials and Methods. (d) MDA-MB-213-1833 cells were incubated for 48 h in the presence or absence of thymoquinone (1 and 10 μM), LY (20 μM) onto an Oris cell invasion assay plate. Cell invasion images were acquired by inverted microscope as described in Materials and Methods. Experiments were repeated at least three times. Columns, mean; bars, SEM. **Significantly different at $P < 0.01$, ***Significantly different at $P < 0.001$.

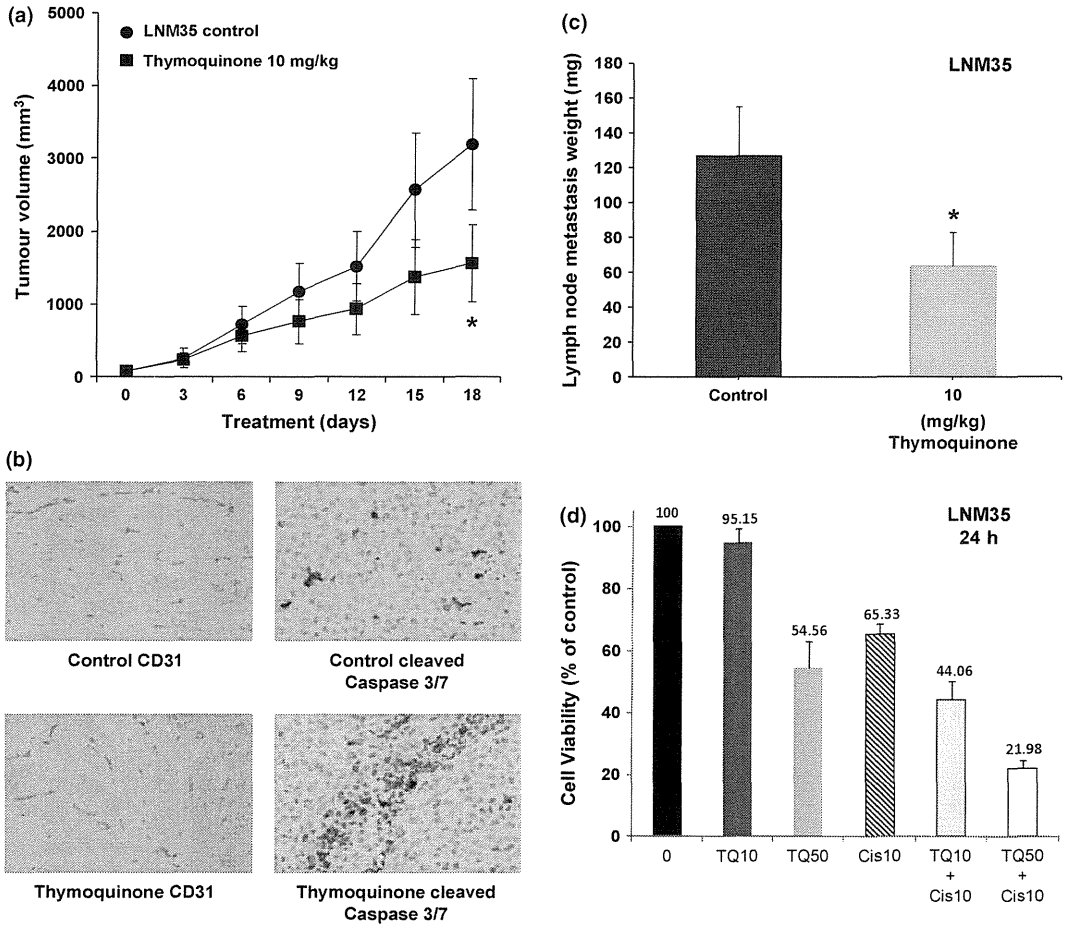

Figure 5 Impact of thymoquinone on the tumor volume, angiogenesis, cancer cell death, and metastasis of established human lung cancer xenografts. (a) Nude mice were xenografted S.C. with human lung LNM35 cancer cells (10^6 cells per animal) and treated with thymoquinone (10 mg/kg, i.p) or control (carrier solution alone) 3 days per week (Sunday, Tuesday, and Thursday) for a total of 18 days. Data points represent the mean ± SEM of 6 to 7 mice per group. Statistically significant differences are indicated in (a) for tumor volume (*$P < 0.05$ vs. control). (b) Immunohistochemical staining for CD31 (right panel) and cleaved caspase-3/7 (left panel) in LNM35 human lung cancer growing in nude mice treated with saline (control) and thymoquinone. (c) Lymph nodes metastasis weight of established human lung cancer xenografts treated with TQ 10 mg/kg for 18 days. *Columns*, mean; *bars*, SEM. (d) LNM35 cells were incubated in the presence or absence of thymoquinone (10 and 50 μM), cisplatin (10 μM) or with combined thymoquinone and cisplatin treatment for 24 h. Cell viability was measured as described in Materials and Methods. All experiments were repeated at least three times. *Columns*, mean; *bars*, SEM.

line LNM35 by examining axillary lymph nodes. In the control-treated group, the mean lymph nodes weight was 127 ± 28.1 mg compared with 63.5 ± 19.2 mg in the groups treated with TQ 10 mg/kg/day for 18 days (*Figure 5c*).

Thymoquinone synergizes with cisplatin to inhibit cellular viability

Our *in vivo* data encouraged us to investigate the possible contribution of TQ to enhance the cytotoxicity of cisplatin in the human NSCLC lung cell line LNM35 in vitro. Interestingly, low to moderate concentrations of TQ (10 and 50 μM) revealed a synergistic inhibition of LNM35 cell viability in vitro in combination with cisplatin (10 μM) (*Figure 5d*).

An attempt to identify a target for thymoquinone

In an attempt to suggest possible targets for thymoquinone, we carried out a short chemo-informatics study combining a reverse docking procedure and a ligand-based similarity approach. In the former approach, we used the TarFisDock web server to reverse dock TQ on

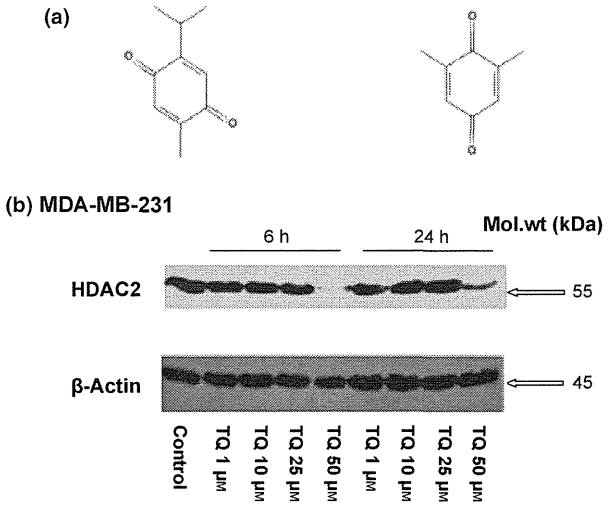

Figure 6 (a) 2D sketches of THQ (Left) and 2, 6-dimethyl-1, 4-benzoquinone (Right) that have a 0.84 pairwise Tanimoto coefficient. (b) MDA-MB-231 cells were exposed to increasing concentrations of TQ, and total proteins were collected after 6 and 24 h, and the expression of HDAC2 protein was assessed by immunoblot.

1207 different protein structures. This corresponds to 841 different protein targets spanning through a vast array of protein types and associated diseases. Among the results, we found several potential targets for TQ that are known to be involved cancer, such as Carboxypeptidase A (Pancreatic Cancer), Thymidine Kinase (Bladder Cancer), HDAC-2 (Colon Cancer), and Nuclear Vitamin D Receptor (Colorectal and Prostate Cancer). In the ligand-based similarity approach, we used the PubChem server to detect similar compounds to TQ (Tanimoto index above 0.8), and we analyzed the PubChem BioAssay results available for those compounds. Interestingly, only one compound, 2, 6-dimethyl-1, 4-benzoquinone (*Figure 6a*) has been identified as active within a PubChem Bioassay whose protein target was clearly identified (Pubchem Bioassay AID388). The associated target is the human 15-hydroxyprostaglandin dehydrogenase (HPGD). In this context, we demonstrated that TQ treatment for 6 and 24 h resulted in a significant inhibition of HDAC2 proteins (*Figure 6b*).

DISCUSSION

Nigella sativa popularly known as black seed has been used in traditional medicine for the treatment of a variety of illnesses, including bronchial asthma, headache, dysentery, infections, obesity, back pain, hypertension, gastrointestinal problems, and eczema [4]. Several bioactive components of black seed have been identified, including thymoquinone, thymol, thymohydroquinone, and dithymoquinone. Among them thymoquinone (TQ) has been reported to exhibit antioxidant, anti-inflammatory, and chemopreventive effects [3,4,12].

Results presented in this study demonstrate that thymoquinone induces cell death of several human cancer cell lines derived from lung, liver, colon, melanoma, and breast cancer. These results are in line with several other studies that have demonstrated that thymoquinone induced apoptosis in cancer cell lines including myeloblastic leukemia, pancreatic, ovarian, breast and colorectal adenocarcinoma [4,5,13–15].

Previous studies reported that thymoquinone induced apoptosis in tumor cells by suppressing COX-2, survivin, Bcl family proteins, STAT3 phosphorylation, NF-κB, Akt activation, extracellular signal-regulated kinase (ERK), and inhibition of telomerase activity leading to telomere shortening [6,12,16–19]. A recent study proposed a new mechanism for the antineoplastic effect of TQ. The authors demonstrate that treatment with TQ induced ROS generation, which increased JNK and ERK in an attempt to bypass the stress injury. However, ERK and JNK fail to confer a survival role, and the cells undergo apoptosis [20].

It has been reported that Akt activation may allow cells to evade the deleterious consequences of DNA damage, and consequently, the inhibition of Akt phosphorylation will markedly enhance DNA damage [21]. The γ-H_2aX, phosphorylated histone H_2AX, formation is an early chromatin modification event that follows initiation of DNA fragmentation during apoptosis before DNA repair. We present strong evidence that the antineoplastic effect of TQ is at least in part, associated with induction of the DNA damage protein H_2aX in both breast and lung cancer cells. These results are in line with similar finding in colon cancer cells [22]. In this context, we provided mechanistic evidences that TQ-induced cell death is mediated, at least in part, by inhibition of the phosphorylation of the survival serine threonine kinase Akt leading to phosphorylation of γ-H_2aX.

Induction of apoptosis is a key factor in the response of tumors to chemotherapy. Cells can respond to DNA damage either by undergoing cell cycle arrest, to facilitate DNA repair, or by undergoing cell suicide. Apoptosis is a major form of cell death involving the

mitochondria (intrinsic pathway) or death receptors (extrinsic pathway). The intrinsic pathway involves the release of cytochrome *c* from the intermembrane space of the mitochondria leading to the activation of downstream caspase-3/7 that leads to the cleavage of PARP and the death response [23]. In this context, we determined the nature of cell death induced by TQ in our cancer cells, which engages the mitochondrial pathway, allowing the release of cytochrome *c*. Our results also show that TQ activates the apoptotic pathway, as evidenced by the activation of caspase-3/7, the main effector of apoptosis. These results are in line with previous studies indicating that caspase-3 activation-mediated the TQ-induced apoptosis in myeloblastic leukemia HL-60 cells and human laryngeal carcinoma cells HEp-2 [15,24]. Caspase-3 recognizes the DEVD motif within the amino-terminal domain of PARP-1 and cleaves this nuclear enzyme between amino acids 214 and 215 [25]. In this study, a p85 protein band representing the caspase-3 cleaved PARP-1 was generated in HepG2 cells after exposure to TQ.

In this study, we reported that treatment with non-toxic concentrations of thymoquinone (0.01, 0.1 and 1 μM) inhibits the invasiveness of human lung cancer cells LNM35 and human mammary adenocarcinoma cells (MDA-MB-231 and MDA-MB-213-1833). This ability of low concentration of TQ (0.1–10 μM) to reduce the invasiveness of breast cancer cells was also reported recently [26]. In line with our results, recent studies indicated that thymoquinone exhibits significant inhibitory effect on HGF-induced HepG2 hepatoma cell motility and invasion; VEGF-induced PC3 prostate cancer cell motility, on human umbilical vein endothelial cell (HUVEC) motility and invasion and also glioblastoma cells associated with FAK, MMP-2, and MMP-9 downregulation [17,27]. Similarly, high concentration of TQ (20–80 μM) significantly inhibits mouse C26 colon cancer cell invasion, pancreatic cancer cell invasion and metastasis as well as human NCI-H460 lung cancer cell invasion [28]. Taken together, these results confirm that the impact of thymoquinone on cancer cell motility and invasion is not tissue specific and suggests a potent antimetastatic effect of TQ. In this context, we demonstrated that TQ significantly reduces metastasis *in vivo*.

The chemotherapeutic agents currently in use for lung cancer are still unsatisfactory because of associated co-lateral toxicity and drug-induced resistance that encouraged us to investigate *in vivo* the anticancer activity of thymoquinone in athymic mice xenografted with the LNM35 human lung cells. Previous reports have demonstrated that the LD50 of TQ after intraperitonial injection to mice were 104.7 mg/kg [29]. A phase I study conducted by Al-Amri and Bamosa had reported no significant systemic toxicities in adult patients with solid tumors or hematological malignancies who were treated with thymoquinone [30]. It was also found that the human body could tolerate a dose of thymoquinone up to 2600 mg/day [3]. We demonstrated that intraperitonial administration of thymoquinone (10 mg/kg, 10 times less that the LD50 dose) for 18 days slows down LNM35 lung tumor growth by 39% without manifest side effects. It has also been demonstrated previously that thymoquinone (10 mg/kg) does not induce mortality or any pathological abnormalities in the lung, heart, or kidneys [31]. Our findings are in agreement with other studies showing that TQ (5–20 mg/kg/day) inhibits growth of HCT116 colon cancer and PC3 prostate cancer xenografts [17,28,32]. To determine the mechanism by which thymoquinone inhibits tumor growth, we investigated the impact of this compound on tumor cell survival and angiogenesis using cleaved caspases-3 and CD31 antibodies, respectively. We found that the tumor growth inhibition was associated with significant increase in apoptosis as reported in colon cancer xenografts treated with TQ [28], in contrast with previous report related to potential antiangiogenic effect of TQ [17]. In this study, the antineoplastic effect of TQ does not appear to be due to the inhibition of angiogenesis. At least at the dose of TQ used, no significant difference in neo-angiogenesis was observed between TQ and control LNM35 tumor xenografts.

Clinical trials revealed that single agent treatments rarely result in clinical benefits to cancer patients, suggesting that combination therapy is necessary for effective treatment for majority of cancers. Emerging evidence demonstrates that thymoquinone in combination with gemcitabine and/or oxaliplatin is superior as an antitumor agent compared with either agent alone [16]. It has been reported that TQ potentiates the antitumor activity of cisplatin and improves its therapeutic index in Ehrlich ascites carcinoma and also reduces the toxic effects of various anticancer drugs including cisplatin and doxorubicin [33,34]. Cisplatin is widely used in the treatment of lung, bladder, ovarian, and cervical cancer [35]. The first-line chemotherapeutic protocol in lung cancer is cisplatin in combination with paclitaxel, docetaxel, vinorelbine, gemcitabine, or irinotecan [36]. We examined the

possibility to enhance lung cancer cell death of cisplatin by combination with TQ. Our in vitro data indicate that combination of TQ and cisplatin caused greater inhibition of LNM35 lung cancer cell viability than each drug given alone. Recent study also showed a synergism between TQ and cisplatin in inhibition of the NCI-H460 lung cell proliferation as well as tumor growth [31]. Building on aforementioned results, which strongly support better killing of lung cancer cells when exposed to both cisplatin and thymoquinone, we will evaluate in future plan the therapeutic advantage of combination of cisplatin and thymoquinone in nude mice bearing LNM35 xenografts.

Interestingly, the identification of HDAC-2 among the potential protein targets and the demonstration in this study that TQ treatment leads to a decrease in HDAC2 protein level corroborates the recent findings suggesting that TQ inhibits histone deacetylase (HDAC) activity and induces histone hyperacetylation [37]. On the other hand, the human 15-hydroxyprostaglandin dehydrogenase (HPGD) is a target that has been recently associated with higher risk for colorectal cancer [38], and it is now known that TQ can inhibit tumor growth in murine colon cancer models [28]. Taken together, these preliminary results suggest several potential targets (mainly HDAC proteins and HPGD) and seem to corroborate the previously published studies on the effect of TQ cancer progression.

In conclusion, we provide evidence that TQ induces cancer cell death at least in part via inhibition of Akt phosphorylation leading DNA damage and activation of the mitochondrial-signaling proapoptotic pathway. Furthermore, TQ is also able to reduce the invasiveness of cancer cells and to sensitize LNM35 cancer cells to the cytotoxic effects of the DNA-damaging agent cisplatin. We also report an anticancer effect of TQ in a highly aggressive human lung cancer xenograft in nude mice. Recent study presented preliminary evidence for novel synthetic TQ analogs with biological activity that is better than the parental TQ without systemic toxicity [39]. In view of the available experimental findings, we contend that thymoquinone and /or its analogues may have a strong clinical potential as an anticancer drug either alone or in combination with some chemotherapeutic agents such as cisplatin.

ACKNOWLEDGEMENTS

This work was financially supported by the Research Affairs at the UAE University under a contract no. 02-04-8-11/07 and by Terry Fox Fund for Cancer Research to samir Attoub and haider Raza. The authors wish to thank Ms. Anne John and Ms. Manjusha Sudhadevi, Dept. of Pathology, Ms. Annie John, Dept. of Biochemistry FMHS for their excellent technical help. We thank Prof. Joan Massague from Howard Hughes Medical Institute for providing the MDA-MB-231 and MDA-MB-231-1833 cells and Dr. Mien-Chie Hung from University of Texas MD Anderson Cancer Center for providing the MDA-MB-435 cells.

REFERENCES

1 Parkin D.M., Bray F., Ferlay J., Pisani P. Global cancer statistics, 2002. CA Cancer J. Clin. (2005) **55** 74–108.
2 Gali-Muhtasib H., Roessner A., Schneider-Stock R. Thymoquinone: a promising anti-cancer drug from natural sources. Int. J. Biochem. Cell Biol. (2006) **38** 1249–1253.
3 Woo C.C., Kumar A.P., Sethi G., Tan K.H. Thymoquinone: potential cure for inflammatory disorders and cancer. Biochem. Pharmacol. (2011) **83** 443–451.
4 Gali-Muhtasib H., Diab-Assaf M., Boltze C., et al. Thymoquinone extracted from black seed triggers apoptotic cell death in human colorectal cancer cells via a p53-dependent mechanism. Int. J. Oncol. (2004) **25** 857–866.
5 Rooney S., Ryan M.F. Effects of alpha-hederin and thymoquinone, constituents of *Nigella sativa*, on human cancer cell lines. Anticancer Res. (2005) **25** 2199–2204.
6 Gurung R.L., Lim S.N., Khaw A.K., Soon J.F., Shenoy K., Mohamed Ali S. et al. Thymoquinone induces telomere shortening, DNA damage and apoptosis in human glioblastoma cells. PLoS ONE (2010) **5** e12124.
7 Kozaki K., Miyaishi O., Tsukamoto T., Tatematsu Y., Hida T., Takahashi T. Establishment and characterization of a human lung cancer cell line NCI-H460-LNM35 with consistent lymphogenous metastasis via both subcutaneous and orthotopic propagation. Cancer Res. (2000) **60** 2535–2540.
8 Raza H., Prabu S.K., Robin M.A., Avadhani N.G. Elevated mitochondrial cytochrome P450 2E1 and glutathione S-transferase A4-4 in streptozotocin-induced diabetic rats: tissue-specific variations and roles in oxidative stress. Diabetes (2004) **53** 185–194.
9 Raza H., John A. 4-hydroxynonenal induces mitochondrial oxidative stress, apoptosis and expression of glutathione S-transferase A4-4 and cytochrome P450 2E1 in PC12 cells. Toxicol. Appl. Pharmacol. (2006) **216** 309–318.
10 Li H., Gao Z., Kang L., Zhang H., Yang K., Yu K. et al. TarFisDock: a web server for identifying drug targets with docking approach. Nucleic Acids Res. (2006) **34** W219–W224.
11 Gao Z., Li H., Zhang H., Liu X., Kang L., Luo X. et al. PDTD: a web-accessible protein database for drug target identification. BMC Bioinformatics (2008) **9** 104.

12 Sethi G., Ahn K.S., Aggarwal B.B. Targeting nuclear factor-kappa B activation pathway by thymoquinone: role in suppression of antiapoptotic gene products and enhancement of apoptosis. Mol. Cancer Res. (2008) **6** 1059–1070.
13 Worthen D.R., Ghosheh O.A., Crooks P.A. The in vitro anti-tumor activity of some crude and purified components of blackseed, *Nigella sativa* L. Anticancer Res. (1998) **18** 1527–1532.
14 Shoieb A.M., Elgayyar M., Dudrick P.S., Bell J.L., Tithof P.K. In vitro inhibition of growth and induction of apoptosis in cancer cell lines by thymoquinone. Int. J. Oncol. (2003) **22** 107–113.
15 El-Mahdy M.A., Zhu Q., Wang Q.E., Wani G., Wani A.A. Thymoquinone induces apoptosis through activation of caspase-8 and mitochondrial events in p53-null myeloblastic leukemia HL-60 cells. Int. J. Cancer (2005) **117** 409–417.
16 Banerjee S., Kaseb A.O., Wang Z., Kong D., Mohammad M., Padhye S. et al. Antitumor activity of gemcitabine and oxaliplatin is augmented by thymoquinone in pancreatic cancer. Cancer Res. (2009) **69** 5575–5583.
17 Yi T., Cho S.G., Yi Z., Pang X., Rodriguez M., Wang Y. et al. Thymoquinone inhibits tumor angiogenesis and tumor growth through suppressing AKT and extracellular signal-regulated kinase signaling pathways. Mol. Cancer Ther. (2008) **7** 1789–1796.
18 Li F., Rajendran P., Sethi G. Thymoquinone inhibits proliferation, induces apoptosis and chemosensitizes human multiple myeloma cells through suppression of signal transducer and activator of transcription 3 activation pathway. Br. J. Pharmacol. (2010) **161** 541–554.
19 Arafa e.-S., Zhu Q., Shah Z.I., Wani G., Barakat B.M., Racoma I. et al. Thymoquinone up-regulates PTEN expression and induces apoptosis in doxorubicin-resistant human breast cancer cells. Mutat. Res. (2011) **706** 28–35.
20 El-Najjar N., Chatila M., Moukadem H., Vuorela H., Ocker M., Gandesiri M. et al. Reactive oxygen species mediate thymoquinone-induced apoptosis and activate ERK and JNK signaling. Apoptosis (2010) **15** 183–195.
21 Xu N., Hegarat N., Black E.J., Scott M.T., Hochegger H., Gillespie D.A. Akt/PKB suppresses DNA damage processing and checkpoint activation in late G2. J. Cell Biol. (2010) **190** 297–305.
22 Gali-Muhtasib H., Kuester D., Mawrin C., Bajbouj K., Diestel A., Ocker M. et al. Thymoquinone triggers inactivation of the stress response pathway sensor CHEK1 and contributes to apoptosis in colorectal cancer cells. Cancer Res. (2008) **68** 5609–5618.
23 Fesik S.W. Promoting apoptosis as a strategy for cancer drug discovery. Nat. Rev. Cancer (2005) **5** 876–885.
24 Rooney S., Ryan M.F. Modes of action of alpha-hederin and thymoquinone, active constituents of *Nigella sativa*, against HEp-2 cancer cells. Anticancer Res. (2005) **25** 4255–4259.
25 Wesierska-Gadek J., Gueorguieva M., Wojciechowski J., Tudzarova-Trajkovska S. In vivo activated caspase-3 cleaves PARP-1 in rat liver after administration of the hepatocarcinogen N-nitrosomorpholine (NNM) generating the 85 kDa fragment. J. Cell. Biochem. (2004) **93** 774–787.
26 Woo C.C., Loo S.Y., Gee V., Yap C.W., Sethi G., Kumar A.P. et al. Anticancer activity of thymoquinone in breast cancer cells: possible involvement of PPAR-γ pathway. Biochem. Pharmacol. (2011) **82** 464–475.
27 Kolli-Bouhafs K., Boukhari A., Abusnina A., Velot E., Gies J.P., Lugnier C. et al. Thymoquinone reduces migration and invasion of human glioblastoma cells associated with FAK, MMP-2 and MMP-9 down-regulation. Invest. New Drugs (2011).
28 Gali-Muhtasib H., Ocker M., Kuester D., Krueger S., El-Hajj Z., Diestel A. et al. Thymoquinone reduces mouse colon tumor cell invasion and inhibits tumor growth in murine colon cancer models. J. Cell Mol. Med. (2008) **12** 330–342.
29 Al-Ali A., Alkhawajah A.A., Randhawa M.A., Shaikh N.A. Oral and intraperitoneal LD50 of thymoquinone, an active principle of *Nigella sativa*, in mice and rats. J. Ayub Med. Coll. Abbottabad (2008) **20** 25–27.
30 Al-Amri A.M., Bamosa A.O. Phase I safety and clinical activity study of thymoquinone in patients with advanced refractory malignant disease. Shiraz E-Med. J. (2009) **10** 107–111.
31 Jafri S.H., Glass J., Shi R., Zhang S., Prince M., Kleiner-Hancock H. Thymoquinone and cisplatin as a therapeutic combination in lung cancer: in vitro and in vivo. J. Exp. Clin. Cancer Res. (2010) **29** 87.
32 Kaseb A.O., Chinnakannu K., Chen D., Sivanandam A., Tejwani S., Menon M. et al. Androgen receptor and E2F-1 targeted thymoquinone therapy for hormone-refractory prostate cancer. Cancer Res. (2007) **67** 7782–7788.
33 Badary O.A., Nagi M.N., al-Shabanah O.A., al-Sawaf H.A., al-Sohaibani M.O., al-Bekairi A.M. Thymoquinone ameliorates the nephrotoxicity induced by cisplatin in rodents and potentiates its antitumor activity. Can. J. Physiol. Pharmacol. (1997) **75** 1356–1361.
34 Nagi M.N., Mansour M.A. Protective effect of thymoquinone against doxorubicin-induced cardiotoxicity in rats: a possible mechanism of protection. Pharmacol. Res. (2000) **41** 283–289.
35 Ferraldeschi R., Baka S., Jyoti B., Faivre-Finn C., Thatcher N., Lorigan P. Modern management of small-cell lung cancer. Drugs (2007) **67** 2135–2152.
36 Lally B.E., Urbanic J.J., Blackstock A.W., Miller A.A., Perry M.C. Small cell lung cancer: have we made any progress over the last 25 years? Oncologist (2007) **12** 1096–1104.
37 Chehl N., Chipitsyna G., Gong Q., Yeo C.J., Arafat H.A. Anti-inflammatory effects of the *Nigella sativa* seed extract, thymoquinone, in pancreatic cancer cells. HPB (Oxford) (2009) **11** 373–381.
38 Hoeft B., Linseisen J., Beckmann L., Müller-Decker K., Canzian F., Hüsing A. et al. Polymorphisms in fatty-acid-metabolism-related genes are associated with colorectal cancer risk. Carcinogenesis (2010) **31** 466–472.
39 Banerjee S., Azmi A.S., Padhye S., Singh M.W., Baruah J.B., Philip P.A. et al. Structure-activity studies on therapeutic potential of Thymoquinone analogs in pancreatic cancer. Pharm. Res. (2010) **27** 1146–1158.

PLOS ONE

Frondoside A Suppressive Effects on Lung Cancer Survival, Tumor Growth, Angiogenesis, Invasion, and Metastasis

Samir Attoub[1]*, Kholoud Arafat[1], An Gélaude[2], Mahmood Ahmed Al Sultan[1], Marc Bracke[2], Peter Collin[3], Takashi Takahashi[4], Thomas E. Adrian[5], Olivier De Wever[2]

1 Department of Pharmacology & Therapeutics, Faculty of Medicine & Health Sciences, U. A. E. University, Al-Ain, United Arab Emirates, **2** Laboratory of Experimental Cancer Research, University Hospital, Gent, Belgium, **3** Coastside Bio Resources, Stonington, Maine, United States of America, **4** Division of Molecular Carcinogenesis, Center for Neurological Diseases and Cancer, Nagoya University Graduate School of Medicine, Nagoya, Japan, **5** Department of Physiology, Faculty of Medicine & Health Sciences, U. A. E. University, Al-Ain, United Arab Emirates

Abstract

A major challenge for oncologists and pharmacologists is to develop less toxic drugs that will improve the survival of lung cancer patients. Frondoside A is a triterpenoid glycoside isolated from the sea cucumber, *Cucumaria frondosa* and was shown to be a highly safe compound. We investigated the impact of Frondoside A on survival, migration and invasion *in vitro*, and on tumor growth, metastasis and angiogenesis *in vivo* alone and in combination with cisplatin. Frondoside A caused concentration-dependent reduction in viability of LNM35, A549, NCI-H460-Luc2, MDA-MB-435, MCF-7, and HepG2 over 24 hours through a caspase 3/7-dependent cell death pathway. The IC50 concentrations (producing half-maximal inhibition) at 24 h were between 1.7 and 2.5 μM of Frondoside A. In addition, Frondoside A induced a time- and concentration-dependent inhibition of cell migration, invasion and angiogenesis *in vitro*. Frondoside A (0.01 and 1 mg/kg/day i.p. for 25 days) significantly decreased the growth, the angiogenesis and lymph node metastasis of LNM35 tumor xenografts in athymic mice, without obvious toxic side-effects. Frondoside A (0.1–0.5 μM) also significantly prevented basal and bFGF induced angiogenesis in the CAM angiogenesis assay. Moreover, Frondoside A enhanced the inhibition of lung tumor growth induced by the chemotherapeutic agent cisplatin. These findings identify Frondoside A as a promising novel therapeutic agent for lung cancer.

Citation: Attoub S, Arafat K, Gélaude A, Al Sultan MA, Bracke M, et al. (2013) Frondoside A Suppressive Effects on Lung Cancer Survival, Tumor Growth, Angiogenesis, Invasion, and Metastasis. PLoS ONE 8(1): e53087. doi:10.1371/journal.pone.0053087

Editor: Srikumar P. Chellappan, H. Lee Moffitt Cancer Center & Research Institute, United States of America

Received June 13, 2012; **Accepted** November 27, 2012; **Published** January 8, 2013

Funding: This work was financially supported by the FMHS grant number NP/08/27 (SA), the UAE University grant under a contract no. 01-04-8-11/09 (SA), the Terry Fox Fund for Cancer Research (SA and TA), the UAEU-NRF 09/10 grant number 21MO72 (SA), and the Maine Technology Institute, Gardiner, Maine, USA, and the National Cancer Institute, RAPID Program (PC). The funding agencies had no role in study design, data collection and analysis, decision to publish, or preparation of the manuscript.

Competing Interests: Peter Collin is director, laboratory manager, employee and stock-holder of Coastside Bio Resources, a Maine, USA Corporation. Thomas Adrian and Peter Collin are co-inventors of a United States patent describing Frondoside A and other sea cucumber glycosides as putative anti-cancer agents, and may benefit financially if Frondoside A becomes a drug for human cancers. This does not alter the authors' adherence to all the PLOS ONE policies on sharing data and materials.

* E-mail: samir.attoub@uaeu.ac.ae

Introduction

Lung cancer is the most common form of cancer with one of the highest mortality rates in the world. Targeted therapies for selected subgroups of patients constitute a remarkable progress in the treatment of lung cancer. However, despite these advances, controversies remain, patients die, and a cure remains elusive [1]. Natural compounds are emerging as a new generation of anticancer agents with limited toxicity in cancer patients [2,3]. They can have high value in tumors resistant to classical chemotherapies or resistant to tyrosine kinase inhibitors such as gefitinib

Sea cucumbers have been valued for hundreds of years in the Chinese diet as a food delicacy, as well as a medicine for a wide variety of diseases. In the United States and Canada, sea cucumber tissues are dried, pulverized and encapsulated as nutraceuticals for over-the-counter dietary health supplements, primarily directed at inflammatory conditions in humans and companion animals [4]. Frondoside A is a triterpenoid glycoside isolated from the Atlantic cucumber, *Cucumaria frondosa*. (See [5] for chemical structure). Recent studies demonstrate that low concentrations of Frondoside A inhibit the growth and induced apoptosis of human pancreatic, leukemia and breast cancer cells via caspase activation [6–8].

The chemotherapeutic agents currently in use for lung cancer are still unsatisfactory due to associated co-lateral toxicity and drug-induced resistance [9–11] which motivate our investigation of the impact of Frondoside A on human non-small cell lung cancer survival, migration and invasion *in vitro*, and on tumor growth, metastasis and angiogenesis *in vivo* alone and in combination with cisplatin.